Electrochemical conversion of CO_2 to methane: Process modeling and economics

Bas Tiktak

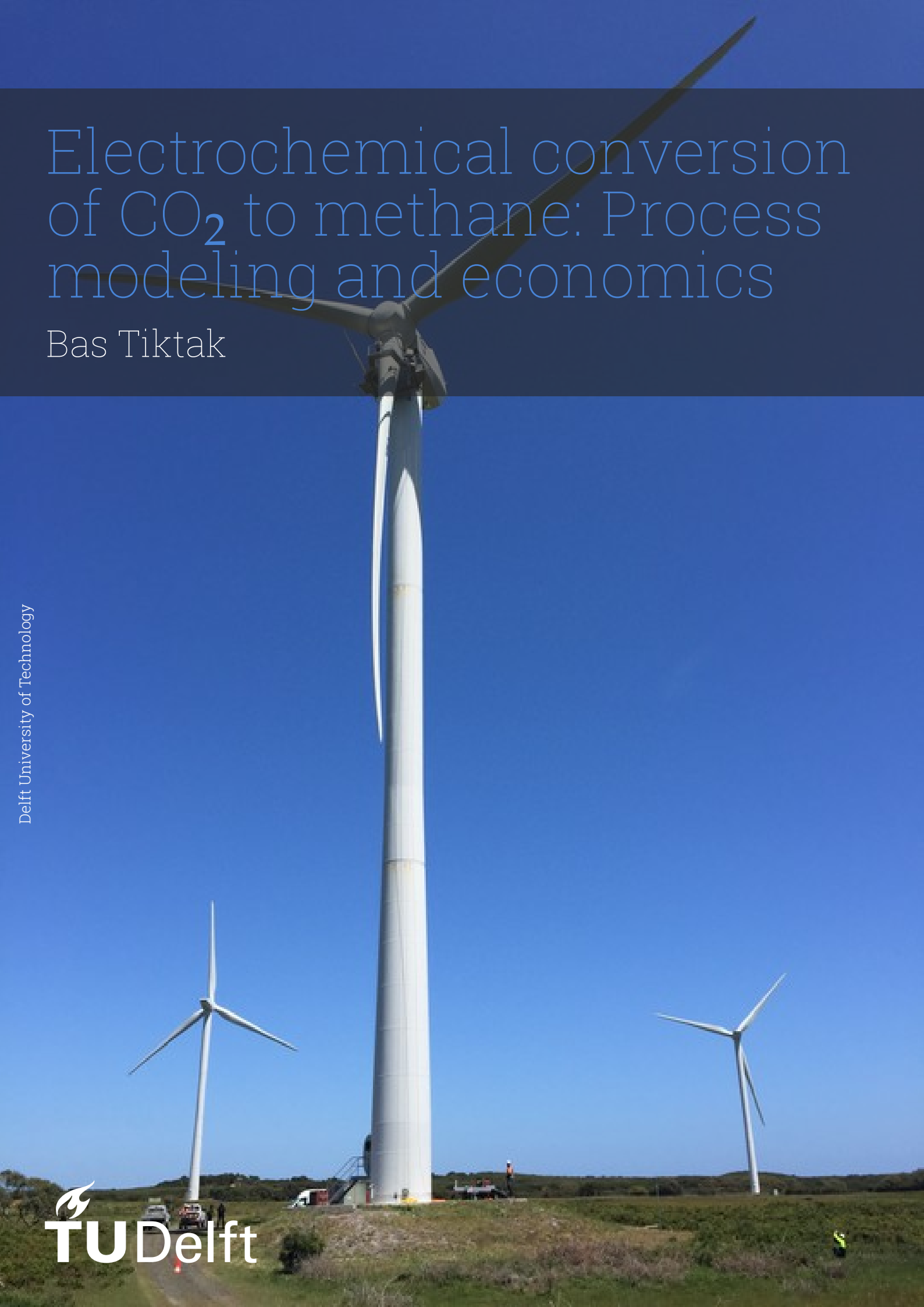

Delft University of Technology

TU Delft

Electrochemical conversion of CO_2 to methane: Process modeling and economics

by

Bas Tiktak

to obtain the degree of Master of Science
in Applied Earth Sciences
at Delft University of Technology,
to be defended publicly on 29.07.2025.

Student number:	4455983
Supervisor:	Dr. Ir. M. Ramdin
Committee:	Dr. H.B. Eral
Faculty:	Faculty of Process and Energy, Delft
Course name:	ME55035 - Final Thesis Energy, Flow, and Process Technology

TU Delft

Abstract

This thesis evaluates the technical and economic feasibility of producing methane (CH_4) via the electrochemical reduction of carbon dioxide (CO_2), offering a pathway to valorize captured CO_2 while integrating surplus renewable electricity into established natural gas infrastructure. A dual-modeling framework was developed: an Excel-based electrolyzer model captures key electrochemical parameters including Faradaic efficiency (FE), current density (CD), cell voltage, and resulting power demand while an ASPEN Plus simulation rigorously models downstream separation, employing cryogenic distillation to achieve high-purity CH_4 and co-products.

The study systematically investigates multiple operational scenarios, reflecting variations in electricity pricing (including projected low-LCOE renewables), CO_2 feedstock costs (derived from different capture strategies), and market values for methane and by-products. A detailed techno-economic assessment quantifies capital expenditure (CAPEX) requirements, dominated by electrolyzer sizing due to constraints on CD and FE, and operational expenditure (OPEX), primarily driven by electricity consumption. Sensitivity analyses reveal that electricity price, electrolyzer CAPEX (tied to CD and cell voltage), and product stream valuations are the most influential parameters affecting the net present value (NPV). Base case simulations show that under current market conditions (25€/MWh electricity, 9,000€/m^2 electrolyzer CAPEX), the process yields a strongly negative NPV. However, scenario analyses demonstrate that moderate improvements across several fronts, reducing cell voltages to 2.5V, increasing CDs beyond 5000 A/m^2, and securing electricity prices under 15€/MWh can collectively transition the process towards economic breakeven within a 30-year project horizon.

Environmental performance was assessed via a simplified CO_2 balance, indicating that for each ton of CH_4 synthesized, approximately 2.75 tons of CO_2 are sequestered. However, this benefit is partially offset by indirect emissions from electricity generation, underscoring the need to combine the process with low-carbon power sources to ensure genuine climate mitigation.

This comprehensive analysis highlights both the promise and the formidable challenges of industrial-scale CO_2 electroreduction to methane. It underscores the critical need for integrated approaches combining advancements in catalyst selectivity and stability (to improve FE toward CH_4), process intensification to achieve higher CDs with minimized overpotentials, and supportive policy mechanisms such as carbon pricing or renewable integration incentives. Ultimately, the findings provide quantitative benchmarks and strategic direction for advancing CO_2-to-CH_4 electrolysis towards economically and environmentally viable deployment.

Preface

I would like to thank everyone who has supported me throughout my graduation project. I am especially grateful for Mahinder Ramdin's guidance and support during this period. Your feedback and advice have been invaluable not only during my studies but also in my professional and personal life.

I would also like to thank Brian Tighe and Marloes Peeters-Reus for their support throughout the graduation process.

Finally, I am deeply thankful to my friends and family, whose unwavering support and encouragement have been irreplaceable throughout my student career.

Bas Tiktak
Delft, July 2025

Contents

1

Introduction

Efforts to mitigate climate change increasingly focus on reducing atmospheric carbon dioxide (CO_2) emissions, the primary driver of anthropogenic global warming. The urgency of this challenge is underscored by international commitments such as the Paris Agreement and the European Union's Green Deal, which aim to achieve net-zero greenhouse gas emissions by mid-century. In this context, Carbon Capture, Utilization, and Storage (CCUS) technologies are viewed as essential tools to complement renewable energy deployment and offset hard-to-abate emissions [Whipple and Kenis 2010, Kortlever et al. 2015].

Among the various CCUS strategies, the electrochemical reduction of CO_2 (CO_2RR) has gained considerable attention in recent years. This process uses renewable electricity to convert CO_2 into value-added chemicals and fuels, effectively coupling carbon recycling with renewable energy integration [Kortlever et al. 2015, Tang et al. 2012, Cave et al. 2018]. As global renewable electricity capacity grows, leveraging surplus power for CO_2 electroreduction could offer a flexible pathway for both grid stabilization and carbon valorization.

Much of the current research on CO_2RR has focused on the production of molecules such as carbon monoxide (CO), formic acid (HCOOH), and ethylene (C_2H_4) [Kortlever et al. 2015,Hung 2020, Blanco et al. 2018]. These products often benefit from relatively favorable reaction kinetics and have well-established markets in the chemical industry. However, the electrochemical production of methane (CH_4) from CO_2 has received comparatively less attention, despite CH_4's large global market size and its direct compatibility with existing natural gas infrastructure for storage, transport, and combustion.

Methane is the primary component of natural gas, widely used for power generation, industrial heating, and as a feedstock in chemical synthesis. Given the existing infrastructure, direct electrochemical conversion of CO_2 to CH_4 provides an opportunity to decarbonize traditional gas applications without requiring extensive system overhaul [Blanco et al. 2018,Singh et al. 2022]. This approach also aligns with power-to-gas concepts, enabling large-scale seasonal energy storage by transforming intermittent renewable electricity into storable chemical energy.

Nonetheless, several scientific and engineering challenges hinder the commercial implementation of CO_2 electrochemical reduction to methane. These include limited catalyst selectivity, low Faradaic efficiencies for CH_4, high overpotentials, and durability concerns that restrict long-term operation [Kortlever et al. 2015,Hung 2020,Jouny et al. 2018a]. Recent advances in electrocatalyst development, particularly involving nanostructured and facet-controlled copper surfaces, have shown promise in enhancing CH_4 selectivity and stability under industrially relevant current densities [Tang et al. 2012,Cave et al. 2018,Hung 2020]. However, these improvements often come at the cost of increased process complexity, requiring precise control over electrolytes, pH, and cell configurations to suppress competing hydrogen evolution reactions.

This thesis aims to explore the technical and economic viability of electrochemical CO_2 reduction to methane under a range of operational scenarios. The study adopts a two-pronged modelling approach: an Excel-based tool estimates key cell performance metrics such as current density, Faradaic efficiency, and power consumption, while an Aspen Plus process simulation models downstream separation and purification requirements. These models are integrated into a techno-economic analysis that assesses feasibility under varying market and policy conditions. Sensitivity and uncertainty analyses further identify the most critical cost drivers, offering insights into pathways for future optimization.

By focusing on methane, this work seeks to fill a gap in the existing literature, providing a comprehensive evaluation of a process that could leverage existing gas infrastructure for rapid decarbonization. The findings aim to inform both industrial stakeholders and policymakers considering investment in next-generation CCUS solutions.

1.1. Societal, Technical, and Economic Relevance

Modelling the overall process of electrochemical CO_2 reduction (CO_2RR) provides crucial insights into the feasibility of scaling up from laboratory experiments to industrial operations. From a technical perspective, such modelling helps evaluate key parameters including Faradaic efficiency, current density, energy consumption, and reactor sizing. By systematically studying these metrics, it becomes possible to identify operational bottlenecks, optimize process conditions, and explore the impact of catalyst performance and cell design on overall system efficiency. Moreover, integrating the electrolysis step with downstream separation and purification units through rigorous process simulation in tools like Aspen Plus allows for an overall assessment of the mass and energy balances required for continuous operation.

The societal implications of advancing electrochemical CO_2RR to methane are substantial. As methane remains the primary component of natural gas, this pathway enables direct integration with existing gas infrastructure for storage, transportation, and end-use. This alignment minimizes the need for extensive modifications to current energy systems, offering a pragmatic route toward decarbonization. By utilizing captured CO_2 to produce a familiar energy carrier, such technologies support circular carbon approaches and can help meet stringent climate targets. In addition, these developments could prompt policymakers to consider stronger CO_2 pricing mechanisms, emissions regulations, or targeted subsidies that accelerate deployment of electrochemical conversion technologies. Public acceptance may also be higher when the technology leverages existing energy systems while visibly contributing to climate goals.

From an economic standpoint, techno-economic modelling clarifies the conditions under which large-scale CO_2 electrolysis could become commercially attractive. This includes analyzing the interplay of electricity costs, CO_2 feedstock pricing, catalyst lifetime, and market prices for methane and by-products. Sensitivity and uncertainty analyses highlight critical cost drivers, helping industry and investors understand financial risks and potential returns. By quantifying metrics such as net present value (NPV) and payback periods under different scenarios, this research provides a foundation for informed decision-making on future investments in electrochemical CO_2 utilization.

In summary, this work not only addresses technical process optimization but also supports broader societal objectives of reducing greenhouse gas emissions, while offering economic insights that are vital for attracting industrial interest and shaping effective policy frameworks.

1.2. Research Questions

This paper will focus on investigating and answering these questions, highlighting any opportunities and challenges that may arise.

"Is there feasibility in the industrial scale methane production through electrochemical reduction of

CO_2?"

"How can we best model the large-scale process plant to create an analysis of the costs?"

These questions pose an inquiry into the future landscape of CO_2 capture and utilization. Finding out in which economic environment producing CH_4 from CO_2 would be possible. As more CO_2 is captured, the costs must be balanced with income and using a method of utilising and then selling the products could open an avenue for corporations to invest in a similar technology. Investments in this large-scale process are large and therefore must be carefully evaluated. The future of this technology depends on scalability, which is only possible with profitability.

2

Literature Review

2.1. Background

The electrochemical reduction of carbon dioxide (CO_2RR) has garnered increasing attention as a route toward sustainable chemical synthesis and energy storage. As the urgency of climate action, researchers and policymakers alike have sought technologies that can effectively valorise CO_2 emissions while integrating with renewable energy systems. Among the spectrum of possible CO_2RR products methane (CH_4) is especially relevant due to its high energy density, ease of storage and compatibility with existing natural gas infrastructure. As noted in recent work, CH_4, as a C1 product, has the highest energy density and is a direct substitute for natural gas [Kortlever et al. 2015].

The central principle of CO_2RR involves reducing gaseous CO_2 into hydrocarbons or oxygenates through a sequence of proton-coupled electron transfers. This inherently multi-step process presents both thermodynamic and kinetic barriers. While several metals have been investigated, copper remains the only monometallic catalyst capable of yielding hydrocarbons and alcohols in meaningful quantities [Tang et al. 2012]. On the other hand, copper suffers from poor selectivity and competition from the hydrogen evolution reaction (HER), especially under high current densities [Cave et al. 2018].

Achieving selective CH_4 production requires careful catalyst design and process control. New approaches involving gas diffusion electrodes, nanostructured catalyst surfaces, and tandem cells have emerged as promising routes to improve methane selectivity [Whipple and Kenis 2010]. However, challenges remain in balancing mass transport, CO_2 access, and proton supply across the catalyst interface.

Membrane electrode assembly (MEA) systems have shown promise for CO_2RR [Verma et al. 2016], particularly in maintaining high current densities and enabling compact system design. Gas diffusion layers (GDLs) in these systems help facilitate efficient reactant delivery and product removal [Hung 2020]. However, issues such as flooding, carbonate formation, and catalyst degradation continue to limit long-term performance.

The intermittency of renewable power sources further complicates the scalability of CO_2RR systems. Dynamic operation can cause fluctuations in product distribution [Jang et al. 2021] and reduce catalyst lifetimes [International Energy Agency 2025]. Consequently, stable operation across varying power inputs is crucial for integrating electrolysis with the grid.

Economically, CO_2RR to methane remains challenged by high capital and operational costs. While electricity is the dominant variable cost [Jouny et al. 2018a], system efficiency, lifetime, and product market value significantly affect feasibility. Policy interventions such as CO_2 taxation or renewable fuel subsidies are often necessary to improve competitiveness [Paltsev et al. 2011].

This thesis builds on these considerations by quantifying the technical and financial viability of CO_2-to-CH_4 conversion using a combined electrochemical and thermodynamic modeling approach. The aim is to inform future development strategies by identifying key levers for process improvement.

2.2. CO_2 Sources

For the implementation of electrochemical CO_2 reduction (CO_2RR), it is essential to analyze potential sources of CO_2. Increasingly, technologies are being deployed to capture CO_2 from industrial emissions. Expanding such capture and storage capabilities will be critical for supplying CO_2 to CO_2RR systems at scale, directly influencing feedstock costs.

2.2.1 Carbon Capture

Driven by global net-zero policies [Hung 2020], efforts to reduce atmospheric CO_2 concentrations have intensified. New carbon capture and storage (CCS) technologies are under development to improve energy efficiency and provide practical climate mitigation pathways [Blanco et al. 2018]. Capture strategies include direct air capture, mobile carbon capture, bioenergy with carbon capture and storage (BECCS), and the use of natural sinks.

Direct Air Capture

Direct air capture extracts CO_2 from ambient air using sorbent materials, producing high-purity CO_2 gas streams [Wilberforce et al. 2019]. Typical systems involve an air collector that draws atmospheric air through a sorbent bed, followed by regeneration to release CO_2 [Terlouw et al. 2021]. However, these systems have high energy demands for releasing CO_2 from the sorbents.

Carbon Capture from Industrial Sources

A major focus is capturing CO_2 directly from industrial point sources [Abdullatif et al. 2023]. Such systems extract CO_2 from fossil fuel combustion processes, achieving removal efficiencies from approximately 10% to 90%, depending on the concentration of the source [Babacan et al. 2020]. While attractive to major emitters, these systems face cost challenges due to their energy-intensive nature [Terlouw et al. 2021].

Pre-combustion methods involve separating CO_2 from natural gas or syngas, typically via gasification or steam reforming, followed by a water-gas shift that produces mainly CO_2 and H_2 [Theo et al. 2016]. The hydrogen can then be combusted for energy, while the CO_2 can be stored or utilized in CO_2RR processes [van der Giesen et al. 2017].

Post-combustion capture extracts CO_2 directly from flue gas, enabling retrofits on existing power plants. However, flue gas desulfurization reduces CO_2 concentrations, complicating capture. Large-scale systems predominantly rely on amine absorption [Peters et al. 2011], although newer approaches explore cryogenic, adsorption, and membrane-based technologies. Due to the corrosive nature of amines, these systems often face challenges in long-term profitability. Increasing CO_2 capture from industrial sources is essential for achieving net-zero targets.

Biogenic CO_2 originates from natural emitters such as plants, trees, and soils, which also sequester carbon through photosynthesis [Harris et al. 2018]. Global land-use and land-cover change (LULC) initiatives enhance CO_2 uptake, complementing engineered solutions.

2.3. Fundamentals of Electrochemical CO_2 Reduction to Methane

Electrochemical CO_2RR uses a cell consisting of a cathode, an anode, and an electrolyte. Reduction of CO_2 occurs at the cathode, while oxidation proceeds at the anode. The choice of electrode is critical for selectivity, efficiency, and overall system performance. Materials such as Ag and Cu are widely studied. Additionally, novel metal-organic frameworks and nanostructured catalysts reduce activation energy, thereby improving efficiency [Zhao et al. 2017]. CO_2RR can yield products including CO, formic acid, methane, ethylene, and various alcohols.

2.3.1 Performance Indicators

Key metrics for CO_2RR include selectivity, Faradaic efficiency (FE), current density, and overpotential. The applied voltage must exceed the thermodynamic potential this excess is the overpotential. High FE indicates selective formation of the target product, governed by the cathode material, electrolyte, and cell design. Current density reflects the reaction rate, with higher values indicating faster production [Kortlever et al. 2015].

Faradaic Efficiency

Faradaic efficiency quantifies the proportion of charge that contributes to forming the desired product:

$$\mathrm{FE} = \frac{n \cdot F \cdot Q}{z \cdot I \cdot t} \tag{2.1}$$

where n is the number of moles produced, F is Faraday's constant, Q is the total charge passed, z is the number of electrons transferred, I is the current, and t is time. A higher FE means more efficient conversion of charge into product relative to competing reactions such as hydrogen evolution (HER).

Current Density

Current density indicates how much current is applied per electrode area and impacts the production rate:

$$j = \frac{M_a \cdot FE \cdot n_A \cdot Q}{t \cdot S} \tag{2.2}$$

where M_a is the moles produced, n_A is the electron transfer number, Q is charge, t is time, and S is the electrode area [Peterson et al. 2010]. Higher current densities enable increased production.

Energetic Efficiency

Energetic efficiency (EE) compares the useful energy output to the total electrical input:

$$EE = \frac{V_{appl} \cdot FE}{V_A} \tag{2.3}$$

whereas the overpotential is given by:

$$\eta = V_{\mathrm{appl}} - V_{\mathrm{ther}} \tag{2.4}$$

Minimizing η is essential for improving EE [Xie et al. 2019].

2.3.2 Electrochemical Reactions at the Cathode and Anode

In the electrochemical reduction of CO_2, distinct reactions occur at the cathode and the anode, each governed by its thermodynamics and kinetics. Understanding these half-cell reactions is essential for optimizing overall system efficiency, selectivity, and long-term stability.

At the cathode, CO_2 is reduced through multiple possible pathways, yielding a variety of products depending on operating conditions such as temperature, pressure, electrolyte composition, and, critically, the catalyst employed [De Jesús-Cardona et al. 2001]. Gold (Au), silver (Ag), and palladium (Pd) are well-known for facilitating the two-electron reduction of CO_2 to CO, achieving Faradaic efficiencies (FE) as high as 90% under optimal conditions [Yang et al. 2019]. These metals stabilize the COOH* intermediate effectively, but generally do not favor further reduction to hydrocarbons.

Copper (Cu), on the other hand, exhibits a unique capability among metallic catalysts to produce more reduced carbon products, including methane and various C_{2+} hydrocarbons. This stems from Cu's moderate binding energy for CO intermediates, which allows adsorbed CO to undergo further proton-electron transfer steps rather than desorbing prematurely [Rendón-Calle et al. 2018]. However, the hydrogen evolution reaction (HER), which proceeds at similar potentials, competes directly with CO_2RR. Thus, careful control of electrolyte pH, catalyst morphology, and applied potential is essential to suppress HER and direct electrons toward CO_2 reduction [Merino-Garcia et al. 2016,Delacourt et al. 2008,Hori 2008,Kimura et al. 2018].

Meanwhile, the anode hosts the oxygen evolution reaction (OER), wherein water is oxidized to generate oxygen gas, releasing protons and electrons required to sustain the cathodic reduction processes. The OER is highly sensitive to electrolyte pH. In alkaline environments, the OER occurs at lower overpotentials, which improves the overall energetic efficiency of the electrolyzer. Conversely, in acidic conditions, achieving comparable rates requires significantly higher overpotentials, increasing energy losses. Catalysts such as iridium oxide (IrO_2) and ruthenium oxide (RuO_2) are commonly employed to reduce these overpotentials in acidic systems, although at the cost of using scarce and expensive noble metals Park et al. 2021].

Minimizing the overall cell overpotential (η) across both electrodes is a critical objective for scaling electrochemical CO_2 reduction. Lower η directly translates to reduced electrical energy input per mole of product, thereby enhancing the process's economic and environmental viability. Thus, the concerted optimization of both cathodic and anodic reactions through judicious choice of catalysts, electrolyte formulation, and operating conditions is fundamental to advancing CO_2RR technologies towards industrial implementation.

2.3.3 Electrolyzer Configurations and Their Scalability

The design of the electrolyzer is a crucial aspect in determining the feasibility and scalability of the electrochemical CO_2 reduction process. Various configurations have been investigated, each with unique advantages and limitations when it comes to mass transport, ion management, operational flexibility, and ultimate suitability for industrial scale-up.

Undivided cells represent the simplest form of electrochemical reactor. They typically consist of two electrodes immersed in the same electrolyte without a physical barrier between the cathode and anode compartments. While undivided cells are straightforward and inexpensive to construct, they suffer from significant drawbacks including the crossover of products and reactants between electrodes, which reduces selectivity and overall Faradaic efficiency. These cells are therefore mainly confined to fundamental laboratory-scale studies where simplicity is advantageous [Merino-Garcia et al. 2016].

H-cells are a common next step for small-scale investigations. In these setups, two chambers are separated by an ion-conducting membrane or a porous separator, enabling better control of ionic transport and limiting the mixing of anodic and cathodic products. Despite their widespread use in research for evaluating catalyst performance, H-cells are inherently batch systems with limited throughput. They are also constrained by low CO_2 solubility in aqueous electrolytes and high ohmic resistances across the membrane, which restrict achievable current densities and increase energy losses. These characteristics make them unsuitable for continuous large-scale production [Hori et al. 1989,Durand et al. 2011,Costentin et al. 2013,Jang et al. 2021,Götz et al. 2016].

A more advanced approach involves membrane electrode assembly (MEA) systems. These reactors

integrate the catalyst layer directly with an ion-exchange membrane (often an anion exchange membrane, AEM), which separates the catholyte and anolyte streams. MEA configurations are designed to minimize the distance ions must travel, thereby reducing ohmic losses and enabling much higher current densities. Recent studies have demonstrated that MEAs can achieve current densities in the range of 200–350 mA/cm^2 with Faradaic efficiencies up to 95% for desired products, significantly outperforming undivided cells and H-cells. Additionally, the enhanced gas-liquid interface and controlled ion transport in MEAs help improve mass transfer and selectivity, which are essential for methane-focused processes [Merino-Garcia et al. 2016,Yang et al. 2019,Liu et al. 2022,Yin et al. 2019,Costentin et al. 2013].

Another category is solid oxide electrolyzers (SOEs), which operate at elevated temperatures typically above 600°C. At these temperatures, the ionic conductivity of the solid electrolyte is high, facilitating very large current densities and enabling efficient conversion of CO_2 to CO or syngas. However, the production of methane in SOEs poses additional challenges due to the thermodynamics and kinetics at such high temperatures, often leading to competing reactions. Moreover, the need for complex thermal integration and materials that can withstand prolonged operation under harsh conditions limits the practical deployment of SOEs for large-scale methane synthesis [Zhang et al. 2021,Lim et al. 2014,Hauch et al. 2020,Zhang et al. 2017,Hori 2008].

In summary, while undivided and H-cells are indispensable for preliminary catalyst testing and mechanistic studies, they fall short in meeting the requirements of industrial-scale operation. MEA-based flow reactors currently stand out as the most promising technology for scalable CO_2 electroreduction to methane, thanks to their high current densities, superior Faradaic efficiencies, and continuous operation capabilities. However, achieving long-term stability and minimizing operational costs remain key targets for ongoing research to realize the commercial viability of such systems.

2.3.4 Methane Production by CO_2 Electroreduction: Catalysts, Efficiency and Challenges

The electrochemical conversion of CO_2 to methane is an attractive pathway due to methane's compatibility with existing infrastructure for storage, distribution, and combustion. However, the relatively low market price of methane, approximately €33/kWh [Zhang et al. 2021], means that exceptionally high process efficiencies are required to achieve economic viability. This necessity drives research towards maximizing Faradaic efficiency (FE), increasing current density, and minimizing energy input per unit of methane produced.

Copper remains the most effective and versatile catalyst for facilitating the multi-electron transfer steps needed to reduce CO_2 to methane. Studies have shown that modifications to copper, such as creating nanotwinned structures, can achieve FE for methane as high as 86% [Möller et al. 2023]. Typical CO_2RR experiments with copper-based catalysts report FE values ranging from 48% to 86% at current densities between 100 and 350 mA/cm^2 [Paltsev et al. 2011,Cai et al. 2021]. These figures highlight the progress made in tailoring catalytic surfaces to favor methane formation over competing reactions like hydrogen evolution or C_2 product formation.

Operating conditions significantly influence the selectivity of methane over other hydrocarbons. Lower temperatures, around 2°C, have been found to favor the formation of CH_4 over C_2H_4, likely due to altered kinetics of the key intermediates [Zhang et al. 2020]. Mechanistically, the reduction proceeds through adsorbed intermediates such as COOH, CHO, and COH, with computational studies indicating that pathways involving COH are energetically more favorable for methane formation than routes passing through CHO. This insight helps guide the design of catalysts that can stabilize specific intermediates to enhance selectivity towards CH_4 [Zhang et al. 2021].

Despite these advances, translating laboratory successes to industrial practice faces substantial hurdles. One major limitation is operational stability. While water electrolysis systems routinely demonstrate lifetimes exceeding 80,000 hours, current CO_2RR systems for methane often degrade within 100 hours of operation [Sánchez et al. 2019]. Catalyst deactivation due to surface reconstruction, oxidation, or poisoning leads to reduced activity and selectivity over time. Additionally, the relatively high

overpotentials required (around 0.17 V vs RHE beyond the thermodynamic minimum) drive up energy consumption, further challenging the economic case Wang et al. 2020].

Another set of challenges arises from the separation and purification steps needed downstream. Given that CO_2RR typically produces a mixture of gases including hydrogen, ethylene, and minor oxygenates, efficient separation becomes essential to deliver pipeline-grade methane. These separations contribute substantially to capital and operating costs, impacting overall techno-economic viability.

In summary, while copper-based systems continue to show promise for selectively reducing CO_2 to methane, significant work remains to improve catalyst durability, enhance process energy efficiency, and optimize downstream separations. Addressing these challenges is critical for advancing CO_2RR from a laboratory curiosity to a scalable industrial technology for producing renewable methane.

3

Methodology

In this chapter the outline of the methods used will be explained. To understand what is needed to set up a complete process from a CO_2 and H_2O feed to the final purified CH_4 end product. In excel there will be an electrolyzer model which will contain all the important calculations regarding the outputs and byproducts produced during the electrolyzer, with all the relevant formulas. Additionally, an ASPEN model will be created focusing on the separation of the byproducts, which will be sold or recycled.

3.1. Process Overview

The process of producing CH_4 from CO_2 requires steps in acquiring the feed, creating the electrolysis reaction, and separating the product streams into single-component outputs. In figure 3.1 there is a flow chart showing the inputs and outputs of the process.

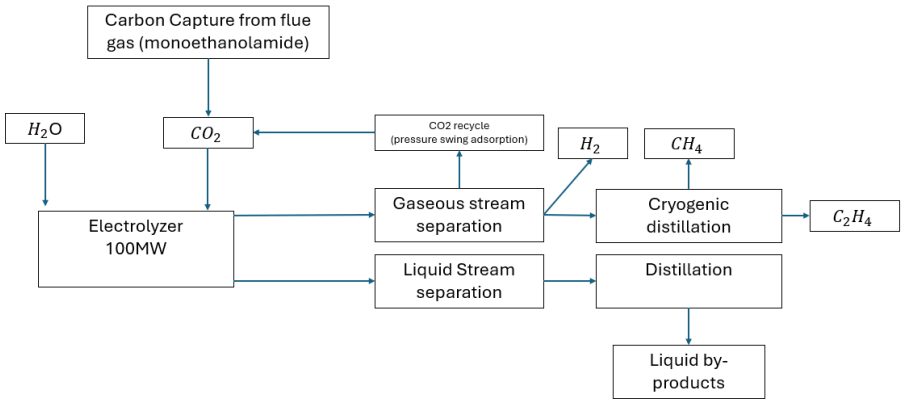

Figure 3.1: Overall overview of the process steps for the process to create CH_4 from CO_2. Starting with using the CO_2 from carbon capture from flue gasses it will enter the process. In this case the input is CO_2 that is already purified. From there, the CO_2 and H_2O are fed into the electrolyser, where the output gases and liquids will then be directed into the specific separation streams, where finally they will be extracted as the pure components.

Designing the process requires the inputs to be defined from the start. One of the first design choices made was the energy input of the electrolyzer. In figure 3.1, it can be seen that there is a 100 MW electrolyzer. Subsequently, this sizes the eletrolyzers cell area, as well as gives the required input of CO_2

and H_2O.

Finding the inputs is an important aspect of the analysis of the scaling of the entire process for a 100 MW electrolyzer. To keep the process as 'green' as possible, it is chosen to take CO_2 only from carbon capture in flue gases and direct air capture. There are differences in the prices of these streams, ranging from 209 to 485 Eur/tonne [Fu and Davis 2023]. From flue gas capture, the prices range from 34 to 85 Eur/tonne [Jiang et al. 2023] through advanced adsorption or technical absorption. H_2O is also specified as an input stream calculated from the conversion ratio and mass balance of the electrolyzer.

The GDE MEA electrolyzer output is determined by the literature and the overall specifications. Furthermore, there is a range of Faradaic efficiencies and current densities found in the literature to be applied and analyzed. Output streams of the electrolyzer are split into two portions. There is the gaseous stream containing the C_2H_6, CH_4, CO_2, and H_2. For the liquid stream, the main components are HCOO-, C_2H_5OH. CH_3COO- n-C_3H_7OH. Separating components in each stream is vital to be able to sell to industries.

Within the electrolyzer the process uses a CU catalyst inside a AEM with CO_2 in gaseous phase at room temperature and pressure. Using the CU(111) with octahedral nanocrystals exposing the 111 facets favours CH_4 production. The total FE of the process can reach 86% in favourable conditions [Cai et al. 2021]. For this paper, the conversion ratio will be taken as 0.6 for the realistic case.

From the electrolyzer the gaseous stream needs to be isolated and separated into the pure components. In this case, there will be an initial separation of the unreacted CO_2. Using pressure swing adsorption the CO_2 is removed. This will not be modelled in ASPEN, but a penalty will be added to the energy and capital investment. Once the CO_2 is removed, the stream containing H_2, CH_4, and C_2H_4 remains. Through an initial compression and cooling stage the H_2 can be removed from the stream using a flash separator, which is possible due to the large difference in boiling points. Subsequently, the CH_4 and C_2H_4 can be removed using cryogenic distillation.

Liquid products play a smaller role in this process as there is not a large mass fraction of liquid products produced. However, the process of separating cannot be ignored in relation to the energy and capital costs. Using a series of distillation columns, these products can be separated and sold at high purities (>99%).

The overall reaction for CO_2 electrolysis is:

$$CO_2 + 8H^+ + 8e^- \rightarrow CH_4 + 2H_2O \tag{3.1}$$

3.1.1 Process Steps

To obtain the CH_4, a considerable number of steps must be done to achieve the desired purity.

1. **Required Feed:** Supplying CO_2 and H_2O at desired ratios and conditions for the 100 MW selected electrolyzer energy input.
2. **Electrochemical conversion:** CO_2 reacts with H_2O in a reactor to form CH_4 and H_2O. Considerable by-products will be made. It can be seen in [EPEX SPOT 2025]. An overview of the by-products is shown in Table 3.1.
3. **CO_2 Recycle :** Due to the conversion ratio, not all the CO_2 will react; therefore, it will need to be separated and reintroduced into the feed stream. A conversion ratio ranging from 0.6 to 0.8 is used [Cai et al. 2021].
4. **Cryogenic cooling:** The gas stream is cooled to enable phase separation of methane.
5. **Cryogenic distillation:** CH_4 is separated from unreacted gases in a distillation column.

Table 3.1: Product distribution over Cu(100) catalyst surface [Jouny et al. 2018a

Product	Faradaic Efficiency (%)
Methane	32.20
Ethylene	28.60
Hydrogen	28.80
Carbon monoxide	3.80
Acetaldehyde	1.40
Ethanol	1.60
Propionaldehyde	1.30
Other gasses	0.30
Inerts	2.00

3.1.2 Governing Equations

The following conservation laws and thermodynamic principles guide the simulation:

Mass balance:

$$\sum \dot{n}_{\text{in},i} = \sum \dot{n}_{\text{out},i} + \dot{n}_{\text{reaction},i} \tag{3.2}$$

Energy balance (steady state):

$$\sum \dot{m}_{\text{in}} h_{\text{in}} + Q = \sum \dot{m}_{\text{out}} h_{\text{out}} \tag{3.3}$$

Phase equilibrium (distillation):

$$y_i = K_i x_i \tag{3.4}$$

where y_i and x_i are the mole fractions of component i in the vapor and liquid phases, respectively, and K_i is the vapor-liquid equilibrium constant.

Heat duty (for cooling and separation):

$$Q = \dot{m} C_p \Delta T \tag{3.5}$$

These equations are implemented within the ASPEN Plus simulation blocks. Sensitivity analyses are performed to evaluate the influence of key parameters such as temperature, pressure, and reactant ratios on conversion efficiency and methane purity.

3.2. Tools and Techniques

The modelling and simulation of the CO_2 electrolysis to methane process, including cryogenic separation, is performed using **ASPEN Plus V12.1**. ASPEN Plus is selected due to its robust physical property database, rigorous thermodynamic solvers, and its capability to simulate chemical reactors and separation units, including cryogenic distillation.

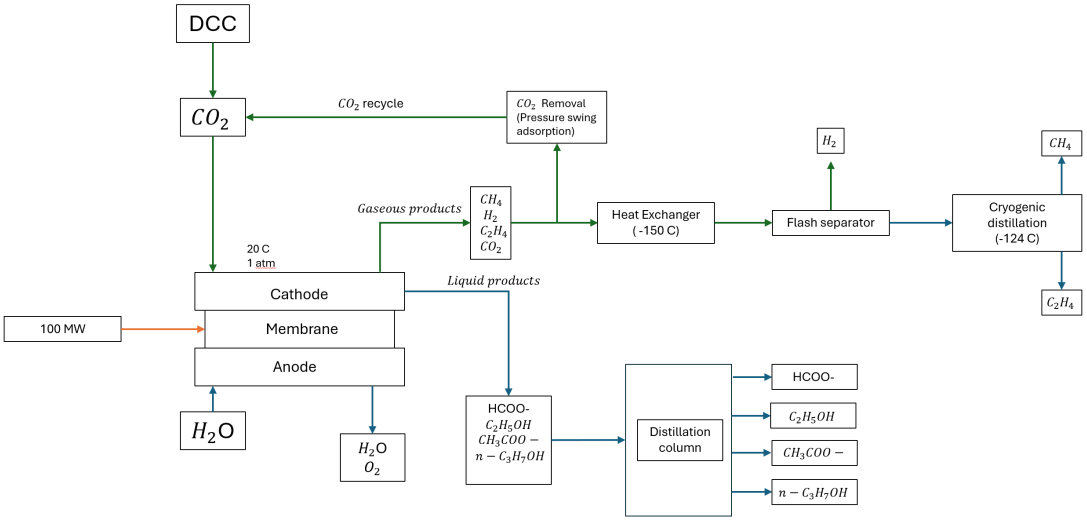

Figure 3.2: In this figure it ca be seen the detailed overview of the process. From the inputs, the electrolyser is fed into the cathode and anode, each releasing outputs. From the cathode, the separation process is initiated, where the gaseous products are removed into their pure forms to be sold. From this stream, there is a recycling of CO_2 that feeds back into the input stream. One method for this separation is pressure swing adsorption. In this paper, the liquid products from the electrolyser are discarded and not taken into account as the output is small.

In figure 3.2 the overall process is depicted, illustrating the steps required to go from the CO_2 from DCC (Direct carbon capture) and to finally create pure CH_4. From the electrolyzer the steps are there to separate the by products. In table 3.2 the products are shown and the fraction. It is important to consider the gaseous and liquid streams that are produced. In the process the focus will be made on the gaseous products. Liquid products have a low FE and are therefore produced in smaller amounts compared to CH_4, H_2, and C_2H_4.

3.2.1 Property Method

The Peng-Robinson equation of state (PENG-ROB) is used as the global property method. This thermodynamic model is suitable for gas-phase systems, especially those involving hydrocarbons and permanent gases at cryogenic conditions.

3.2.2 Component Setup

The following pure by-product components are defined in the simulation:

Table 3.2: Product distribution over Cu(100) catalyst surface

Product	Faradaic Efficiency (%)
H_2	33.00
C_2H_4	5.00
$HCOO^-$	7.00
C_2H_5OH	3.50
CH_3COO^-	1.00
n-C_3H_7OH	0.30

These are selected from ASPEN's standard component databanks. The production of methane via electrochemical CO_2 reduction (CO_2RR) can be estimated from the power input, cell voltage, Faradaic

efficiency (FE), and number of electrons required. The key reaction is:

$$CO_2 + 8H^+ + 8e^- \rightarrow CH_4 + 2H_2O \tag{3.6}$$

This requires $z = 8$ electrons per mole of CH_4 formed. The molar production rate is governed by Faraday's law:

$$\dot{n}_{CH_4} = \frac{\text{FE} \cdot I}{zF} \tag{3.7}$$

where:

- $\dot{n}_{CH_4}$: molar flow rate of CH_4 (mol/s)
- FE : Faradaic efficiency for CH_4 (fraction)
- I : total current (A)
- z : number of electrons per mole of CH_4 (= 8)
- F : Faraday constant (96485 C/mol)

The total current is related to the power input and cell voltage by:

$$I = \frac{P}{V_{\text{cell}}} \tag{3.8}$$

where P is the total electrical power input (W) and V_{cell} is the cell voltage (V).

The electrode area needed can then be calculated from the current density:

$$A = \frac{I}{j} \tag{3.9}$$

where j is the current density (A/m^2).

Finally, the mass flow of methane is given by:

$$\dot{m}_{CH_4} = \dot{n}_{CH_4} \cdot M_{CH_4} \tag{3.10}$$

with $M_{CH_4} = 16$ g/mol.

Calculation with given parameters

Given:

$$\begin{aligned} P &= 100 \text{ MW} = 1.0 \times 10^8 \text{ W} \\ V_{\text{cell}} &= 2.5 \text{ V} \\ \text{FE} &= 33\% = 0.33 \\ z &= 8 \\ F &= 96485 \text{ C/mol} \\ j &= 5000 \text{ A/m}^2 \end{aligned}$$

Total current

From Equation 3.8:

$$I = \frac{P}{V_{\text{cell}}} = \frac{1.0 \times 10^8 \text{ W}}{2.5 \text{ V}} = 4.0 \times 10^7 \text{ A}$$

Methane production rate

From Equation 3.7:

$$\begin{aligned} \dot{n}_{CH4} &= \frac{\text{FE} \cdot I}{zF} = \frac{0.33 \times 4.0 \times 10^7}{8 \times 96485} \\ &= \frac{1.63 \times 10^7}{771880} = 17.05 \,\text{mol/s} \end{aligned}$$

Mass flow of methane

From Equation 3.10:

$$\dot{m}_{\text{CH}_4} = 17.05 \,\text{mol/s} \cdot 16 \,\text{g/mol} = 272.8 \,\text{g/s} = 0.982 \,\text{t/h}$$

Required electrode area

From Equation 3.9:

$$A = \frac{I}{j} = \frac{4.0 \times 10^7}{5000} = 8000 \text{ m}^2$$

A full process design would account for incomplete single-pass conversion and include recycling of unreacted CO_2.

Summary of results

Table 3.3: Key calculated values for 100 MW CO_2 electrolysis to methane

Parameter	Value
Faradaic efficiency (FE_{CH_4})	33%
Power input	100 MW
Cell voltage	2.5 V
Total current	40 MA
Methane production	17.05 mol/s (0.982 t/h)
Electrode area	8000 m^2

This calculation illustrates the scale of reactor infrastructure required to achieve significant methane output. It also underscores the importance of optimizing FE and current density to minimize capital and operational costs.

Mass and Energy Balance for Electrochemical CO_2 Reduction

The process is designed to consume 100 MW of electrical power at a cell voltage of 2.5 V, yielding:

$$I_{\text{total}} = \frac{P}{V} = \frac{100 \times 10^6}{2.5} = 40\,\text{MA} \tag{3.11}$$

The distribution of this current is based on the observed Faradaic efficiencies and conversion ratio:

- 40% to H_2 (hydrogen evolution reaction, HER)
- 60% to CO_2 reduction products

Inside the CO_2 products, current is distributed as:

Table 3.4: Current distribution to individual products.

Product	Share of total current (%)
CH_4	17.0
C_2H_4	5.0
$HCOO^-$	7.0
C_2H_5OH	3.5
CH_3COO^-	1.0
n-C_3H_7OH	0.3

Molar production rates The molar production rate for each species is computed from:

$$\dot{n}_i = \frac{\text{FE}_i \times I_{\text{total}}}{z_i F} \tag{3.12}$$

For CH_4 (8 electrons per molecule):

$$\dot{n}_{\text{CH}_4} = \frac{0.17 \times 40 \times 10^6}{8 \times 96485} = 8.8\,\text{mol}\,\text{s}^{-1} \tag{3.13}$$

Similarly for others:

$$\dot{n}_{\text{C}_2\text{H}_4} = \frac{0.05 \times 40 \times 10^6}{12 \times 96485} = 1.7\,\text{mol}\,\text{s}^{-1} \tag{3.14}$$

$$\dot{n}_{\text{HCOO}^-} = \frac{0.07 \times 40 \times 10^6}{2 \times 96485} = 14.5\,\text{mol}\,\text{s}^{-1} \tag{3.15}$$

$$\dot{n}_{\text{C}_2\text{H}_5\text{OH}} = \frac{0.035 \times 40 \times 10^6}{12 \times 96485} = 1.2\,\text{mol}\,\text{s}^{-1} \tag{3.16}$$

$$\dot{n}_{\text{CH}_3\text{COO}^-} = \frac{0.01 \times 40 \times 10^6}{8 \times 96485} = 0.5\,\text{mol}\,\text{s}^{-1} \tag{3.17}$$

$$\dot{n}_{\text{n}-\text{C}_3\text{H}_7\text{OH}} = \frac{0.003 \times 40 \times 10^6}{18 \times 96485} = 0.07\,\text{mol}\,\text{s}^{-1} \tag{3.18}$$

Mass flow rates

The mass flow rates follow as:

$$\dot{m}_i = \dot{n}_i \times M_i \times 3600 \tag{3.19}$$

Thus for CH_4:

$$\dot{m}_{CH_4} = 8.8 \times 0.016 \times 3600 = 510\,\mathrm{kg\,h^{-1}} \tag{3.20}$$

Repeating for others gives:

Table 3.5: Mass and molar production rates for major products.

Product	$\dot{n}$ (mol/s)	$\dot{m}$ (kg/h)
CH_4	8.8	510
C_2H_4	1.7	170
$HCOO^-$	14.5	660
C_2H_5OH	1.2	200
CH_3COO^-	0.5	150
n-C_3H_7OH	0.07	15

Reactor area estimation

The total reactor area is determined by the average current density j:

$$A = \frac{I_{\text{total}}}{j} \tag{3.21}$$

For example, at $j = 5000\,\mathrm{A\,m^{-2}}$,

$$A = \frac{40 \times 10^6}{5000} = 8000\,\mathrm{m^2} \tag{3.22}$$

This completes the technical mass balance, providing direct inputs for separation train design and economic analysis.

3.3. Data Acquisition and Process Setup in ASPEN Plus

The modelled process is divided into the following key sections: Feed Preparation, Electrochemical Reactor, CO_2 and Hydrogen removal, Cryogenic Pre-Cooling, Cryogenic Distillation Column.

Feed streams are defined using feed blocks with the following conditions:

3.3.1 Electrochemical Reactor

The electrochemical conversion is modelled using an Anion Exchange Membrane (AEM), in Excel. The input parameters are 100 MW, sizing relating to the current density. A higher current density will allow

Table 3.6: Feed Conditions for Electrolyzer System

Parameter	Fresh Feed	Total Feed
Temperature (°C)	20	20
Pressure (bar)	1	1
CO_2 feed rate (kg/hr)	923.52	1847.03
H_2O feed rate (kg/hr)	6191.50	12383.01

Table 3.7: Carbon and Hydrogen Atom Balance per 100 mol Electron Input

Product	FE (%)	e^-/mol	Mol Produced	C Atoms	H Atoms
CH_4	40.84	8	5.11	5.11	20.44
H_2	33.00	2	16.50	0.00	33.00
C_2H_4	5.00	12	0.42	0.84	1.68
$HCOO^-$	7.00	2	3.50	3.50	3.50
C_2H_5OH	3.50	12	0.29	0.58	1.75
CH_3COO^-	1.00	8	0.13	0.26	0.39
n-C_3H_7OH	0.30	18	0.017	0.05	0.14
Total	—	—	—	**10.34**	**60.90**

for a smaller electrolyzer. The conversion ratio and Faradaic efficiencies will have a range of values relating to various current densities [Cai et al. 2021].

In ideal cases the highest FE and current density will be used but other real life scenarios will be simulated. A note is that a higher current density leads to lower FE. This is an important trade of that will be examined.

Table 3.8: Charge, CO_2, and H_2O requirements for CO_2 electroreduction at 40.84% Faradaic efficiency to CH_4.

Parameter	Unit	Value
Total electrons transferred	mol e	90.75
Total charge required	C	8.76×10^6
Total CO_2 consumed	mol	10.34
Total H_2O consumed	mol	45.87

Balancing the chagre to validate the productds is shown in table 3.8 the total charge is calculated from the amount of charge per mol required by the products in table 3.3.1. Using these values, the input stream is then calculated from the production of CH_4, which is the focus. USing the power input and the conversion ratio the feed streams are calculated and shown in table 3.3.

As there is a liquid stream from the electrolyzer will not be examined as it is assumed that due to the low production rate, the separation costs will outweigh the profitability. It would take a large investment to create the distillation columns needed to produce the pure components.

3.3.2 Flash Separator – Hydrogen removal

The use of the flash serparator to remove the H_2 from CH_4 and C_2H_4 is done as this is a relatively easy separation method. Firstly, the stream must be cooled to create a low enough temperature for phase differences. From there, the flash can be utalized to separate the stream. In reality, the flash would not be used, but another distillation or membrane separator.

Table 3.9: Boiling points of main components at 1 bar and approximate values at 10 bar

Component	Chemical Formula	Boiling Point at 1 bar (°C)	Boiling Point at 10 bar (°C)
Hydrogen	H_2	−253	−240
Methane	CH_4	−161	−125
Ethylene	C_2H_4	−104	−70

Hydrogen is to be removed from the stream to be sold and further reduce the gas buildup later in the process. The Flash block operates at a temperature of 133 K and a pressure of 10 bar. Its primary objective is to separate and remove hydrogen (H_2) from the gas stream before it undergoes further cryogenic cooling. This step ensures that hydrogen is efficiently extracted prior to methane purification, enhancing overall process selectivity and energy efficiency.

While increasing pressure raises the boiling points of CH_4 and C_2H_4, it also increases the enthalpy of the feed stream. This additional heat must be removed during cooling, thereby increasing refrigeration duty. Moreover, the marginal gain in phase separation is often outweighed by the nonlinear rise in cooling energy required. Sensitivity analysis confirmed that pressures above 10 bar offered negligible gains in separation performance while imposing a disproportionate increase in refrigeration cost.

3.3.3 Cryogenic Pre-Cooling

Pre-cooling is achieved using a heater block: Costs for cooling were taken from a paper examining the costs for refrigeration [Luyben 2017]. For cooling to -175°C, the price of 218 Eur/GJ, for -150 °C, 115 Eur/GJ and for -50°C, 36 Eur/GJ. It is found that decreasing the temperature exponentially increases refrigeration cost.

Cooling is staged through multiple units. Utilities are used in ASPEN to simulate the cooling energy requirements.

3.3.4 Cryogenic Distillation – DTSWU Column

The separation of methane from the stream containig C_2H_4 is modeled using a `DTSWU` block:

Table 3.10: Distillation Column Design Parameters

Parameter	Value
Feed	Water-free, pre-cooled gas mixture
Number of stages	10–40 (tunable)
Top product	CH_4-rich stream
Operating pressure	1–3 bar

The phase behavior is governed by:

$$y_i = K_i x_i$$

where K_i is the vapor-liquid equilibrium ratio for component i.

3.3.5 Simulation Control and Analysis

The design specifications for the process were carefully selected to achieve the desired methane purity and recovery targets. To assess the performance of the system, a sensitivity analysis was conducted focusing on key parameters. This included variations in reactor temperature and pressure, changes to the reflux ratio within the distillation column, and adjustments in the feed composition. These factors were identified as critical to ensuring optimal separation performance and overall process effectiveness.

Table 3.11: Process Setup in ASPEN Plus for CO_2 Electrolysis to Methane

Unit Operation	**Block Type**	**Main Parameters**
Feed Preparation	FEED	CO_2: 8173 kg/hr, H_2O: 12383 kg/hr T = 298.15 K P = 1–5 bar
Electrochemical Reactor	Excel model	T = 298.15 K, P = 1-2 bar Conversion or equilibrium specified
Hydrogen Separation	FLASH	T = 133 K Removes condensed H_2O
Cryogenic Cooling	COOLER / HEATER	Pre-cooling stages Target T = 110–150 K
Cryogenic Separation	DTSWU	Stages = 20–40 Reflux ratio = 1.3 Feeds pre-cooled gas CH_4 from bottom, unreacted gases from top
Property Method	PENG-ROB	Applied to all units Suitable for cryogenic hydrocarbon systems

3.4. Key Output Parameters

The following performance indicators are collected from the simulation:

Table 3.12: Key Output Parameters

Parameter	Description
Methane production rate	Expressed in mol/s or kg/hr; indicates the quantity of CH_4 produced by the system.
Energy duty	Total energy consumption of the electrochemical and separation units (kW).
CO_2 conversion and CH_4 selectivity	Measures how effectively CO_2 is converted and what fraction of the products is CH_4.
Final methane purity	Mole fraction of CH_4 in the product stream, including composition of byproduct streams.
Overall process efficiency	Efficiency based on the ratio of CH_4 LHV to total electrical input power.

These outputs are used for techno-economic analysis and to assess the viability of the system under different operating and market scenarios. The next chapter presents the results of the simulation and explores process sensitivity and performance trends.

3.5. Scenarios and Assumptions

To evaluate the techno-economic feasibility of electrochemical CO_2 reduction to methane, several key scenarios and assumptions are formulated. These scenarios are grounded in prevailing market dynamics, energy pricing trends, and policy expectations as discussed in the literature.

3.5.1 Electricity Prices

Two electricity pricing schemes are considered: a conventional industrial market and a renewable-surplus scenario. In the general case, electricity prices vary between €0.025/kWh and €0.25/kWh. For surplus-based scenarios, typically during midday hours (12–18h) in summer, prices can drop as low as -€28/MWh. Conversely, in winter, reduced renewable generation raises prices up to €100 to €280/MWh.

3.5.2 Product Price Ranges

The profitability of the process depends on fluctuating product values. The following price ranges are assumed:

Table 3.13: Market Price Ranges for Key Products [Santos et al. 2022,Trading Economics 2025,Pangan and Mulder 2017]

Product	Price Range (€/kg)
CH_4	0.791 to 1.41
H_2	2 to 6
CO_2	-0.050 to 0.1

Based on the experimental data in literature, a Faradaic efficiency (FE) range of 24.1% to 55% is included [Cai et al. 2021]. The FE generally decreases as current density increases, aligning with observations in both PDF studies.

3.5.3 Other Assumptions

Several assumptions are made to simplify the modelling and simulation of the electrochemical and downstream processes. Electrolyzer operations are assumed to occur under ambient conditions of 20°C and 1 atm. The feedstock maintains a molar ratio of H_2O to CO_2 of 4:1, which aligns with literature values used for maintaining hydration and supporting reaction kinetics. Cryogenic separation is assumed to follow membrane-based CO_2 removal and subsequent compression to 10 bar to facilitate low-temperature phase change behaviour.

Unreacted CO_2 is recycled to the system, improving overall conversion efficiency and minimizing waste. Using the value of 22 GJ/tonne CO_2 [Fu and Davis 2023] removed from the gas stream. Liquid extraction steps are omitted to focus the model on gaseous product behaviour, which dominates the CO_2RR process and aligns with the primary interest in methane recovery. Refrigeration cycles are also simplified to reduce model complexity within ASPEN Plus, though they remain representative of realistic energy duties. Lastly, the feed CO_2 is assumed to be of sufficiently high purity and free of contaminants that would otherwise interfere with catalyst activity or process operation.

These assumptions provide the operational and economic boundary conditions [Götz et al. 2016] for all downstream analysis in this thesis.

Table 3.14: Economic and Energy Scenario Ranges Used in Analysis

Parameter	Range
Electricity Price (industrial)	€0.025 to €0.25 /kWh
Electricity Price (renewable summer midday)	€0 to -€28 /MWh
Electricity Price (winter peak)	€100 to €280 /MWh
CH_4 Price	€0.791 to €1.41 /kg
H_2 Price	€2 to €6 /kg
CO_2 Price	€-50 to €500 /tonne
$HCOO^-$ Price	€0.5 to €1.5 /kg
Faradaic Efficiency (FE)	24.1% to 84.1%
Current Density	1000 to 7500 A/m^2
Cell Voltage	1.6 to 3.5 V
CO_2 Separation Cost	€0.02 to €0.06 /kg
Electrolyzer Cost	€4000 to €14000 /m^2
Conversion Ratio	0.4 to 0.8

3.6. Scenarios

To analyse the effects of policies on the possibility of producing methane from CO_2RR, a range of scenarios must be made to ensure that there is a case for the possibilities. Policies regarding carbon tax would be a promising case for the CO_2RR process. Negative energy prices would have a great benefit on the feasibility. Four scenarios have been made: 1. Negative energy prices and carbon tax, 2. Daily operation and carbon tax, 3. Daily operation, no carbon tax, 4. Complete use of 2024 prices. In each of the scenarios, the CH_4 prices will be taken as a range to see the effects on the CAPEX.

3.6.1 Negative energy prices and carbon sourced from a point emitter

This first scenario is considered the best-case scenario. When the prices are negative for both carbon and energy, the government will pay for the reuse of CO_2. As in the literature review, these policies are being considered. However, the negative energy prices are mostly during certain hours of the day, with an average starting from 12 to 18, which limits the hours of operation of the plant.

This scenario will therefore be operational for 6 hours a day, and the energy prices will range from -28 to -100 Eur/MWh. An average price of -68 Eur/MWh will be taken. For the carbon tax, a price range of -50 Eur/kg to -25 Eur/kg is found so an average price of -37.5 Eur/kg is taken. This scenario will also have

the benefit of using renewable energies, so green hydrogen is produced and can be sold for 6 Eur/kg.

3.6.2 Daily operation and CO_2 sources from a point emitter

Secondly, one in which the operation of the plant would not be dictated by the negative energy prices and allow for daily operation. In a year totalling 8000 hours. However, this will have higher energy prices, which range from -100 to 250 Eur/MWh. An average is taken, and 75 Eur/MWh is taken. For the carbon tax value, the same as in the first scenario is taken.

3.6.3 Daily operation and CO_2 is purchased

Thirdly, closer to the real-life economic environment in which the CO_2RR would work. There is no current carbon tax, so companies are not incentivised to pay for the removal of CO_2 from the flue gases. Using these implications, an average price of 150 EUR/tonne is taken and the subsidy is left. In the Netherlands, CO_2 can be sourced commercially from biogenic or industrial emitters at prices ranging from €100 to €200 per tonne. Depending on whether the CO_2 is considered to avoid net emissions, a subsidy of €20 to €50 per tonne may apply, aligning with national decarbonization strategies and EU carbon accounting rules. For this, the price of CO_2 is taken at €150 /tonne.

3.6.4 2024 Prices

Lastly, the average of the energy prices over the year 82 Eur/ MWh [Jouny et al. 2018a] is taken during the operational hours and used in the model. Using this, it will give a projection of what the prospect of running the plant would look like in the current political and economic climate.

4

Results

4.1. Model performance

Applying the setup, assumptions and scenarios to the models, it can be analyzed how a CO_2RR plant would function. Upon exploring the scenarios, it will be seen whether such an industrial-scale plant will have the economic viability for investment. Scenarios depending on the current and future ecopolitical climate will be applied in the four specified scenarios. Graphs showing the outputs, the break-even period, and the sensitivity will accompany the scenarios.

First, the performance and validity of the models must be seen. In the case of the electrolyzer, there must be a correct mass balance and energy balance to satisfy the validity.

4.2. Electrolyzer

A simplified material balance was performed to quantify the input requirements of carbon dioxide (CO_2) and water (H_2O) for the electrochemical reduction process, based on the Faradaic efficiencies (FE) of the various products. The balance assumes a normalized charge input equivalent to 100 moles of electrons to facilitate mole-based accounting.

Given this output distribution and assuming stoichiometric conversion from CO_2 and H_2O, the following input flows are required: Based on the electrochemical model, approximately 10.34 moles of CO_2 are reduced per 100 moles of electron input. Additionally, the protons required for the reduction reaction are met by water, contributing around 60.90 moles of hydrogen atoms, which corresponds to roughly 30.45 moles of H_2O consumed in the process.

These values scale proportionally with the total current applied. For example, at an actual CH_4 production rate of 1847.03 kg/hr and FE = 40.84%, this corresponds to a total CO_2 requirement of approximately 11357.32 kg/hr and H_2O requirement of 75904.70 kg/hr.

4.2.1 Current density and Faradaic efficiency

From the electrolyzer model, an analysis can be made of the effect of the current density and Faradaic efficiency on the performance and costing of the products. Using a range of current densities associated with FE, an analysis can be made of the sizing and the optimal cell voltage needed. A cell voltage of 2.5 V is taken.

Table 4.1: Performance of different operating conditions for CO_2 electrolysis to CH_4

FE (%)	**Current density** ($A\,m^{-2}$)	**Total area** (m^2)	**Output** ($mol\,s^{-1}$)	**Efficiency (%)**
81.7	180	179,211	34.14	27.39
74.2	2,226	14,039	30.04	24.10
60.0	1,350	23,895	25.07	20.12
56.0	7,500	41,667	22.67	18.18
55.2	1,000	312,500	22.34	17.93
48.0	1,120	279,018	22.67	18.19
42.0	1,080	29,869	17.55	14.08
40.8	2,500	125,000	19.43	15.59
24.1	5,000	62,500	16.53	13.27

It can be seen in table 4.1 that there is a correlation between the FE and the overall efficiency. Increasing the FE increases the efficiency but reduces the power density, in turn making a larger electrolyzer. Incorporating the price per m^2 of 9000 EUR/m^2 for the electrolyzer. Illustrating that with the studies found linking the high FE to lower CD it creates a very large area of electrolyzer needed. As the current density is very low for the highest FE, there is a large area required to run the process. It is optimum to have a high FE and CD, increasing efficiency and reducing capital costs, respectively.

4.2.2 Separation

The ASPEN model covers the downstream separation of the gaseous and liquid byproducts. Table 4.1 is an overview of the products produced. These are dependent on the setup of the electrolyser. For this model, simplicity was a key factor to ensure not too much complexity for the distillation columns and the refrigeration cycles.

The performance of the model is dictated by the individual equipment and how it works in unicen. Certain parameters can be changed in the setup of the compressor, flash, heat exchangers, and distillation columns. Sensitivity analysis is done to the pressure of the compressor, the temperature of the flash and the temperatures of the heat exchangers. Analyzing the output streams and the overall energy balance will find the optimal settings for the model.

Alternative separation methods such as pressure swing adsorption (PSA) and membrane technologies were considered, and their ability to separate methane and ethylene from the product gas mixture. PSA systems are generally effective for bulk gas separations and offer relatively low capital and operating costs. However, their selectivity for related low molecular weight species such as CH and CH is limited, often requiring multiple stages and lower product purities. Membrane separation, while compact and energy efficient, suffers from limited selectivity and permeability trade-offs, especially when attempting to separate hydrocarbons with similar properties. However, cryogenic distillation enables separation due to the distinct boiling points of CH (161.5°C) and CH (103.7°C at 1 bar). Although it entails higher energy consumption due to refrigeration, it was selected for this study due to its ability to consistently achieve high product purities.

4.3. ASPEN Model

Below in figure 4.1, the model used for the separation simulation is shown. It includes the gaseous separation stream in the METMIX and the liquid in the L-MIX. For this ultimate study, the liquid separation was not used as it only accounts for a small part of the possible sales and energy consumption.

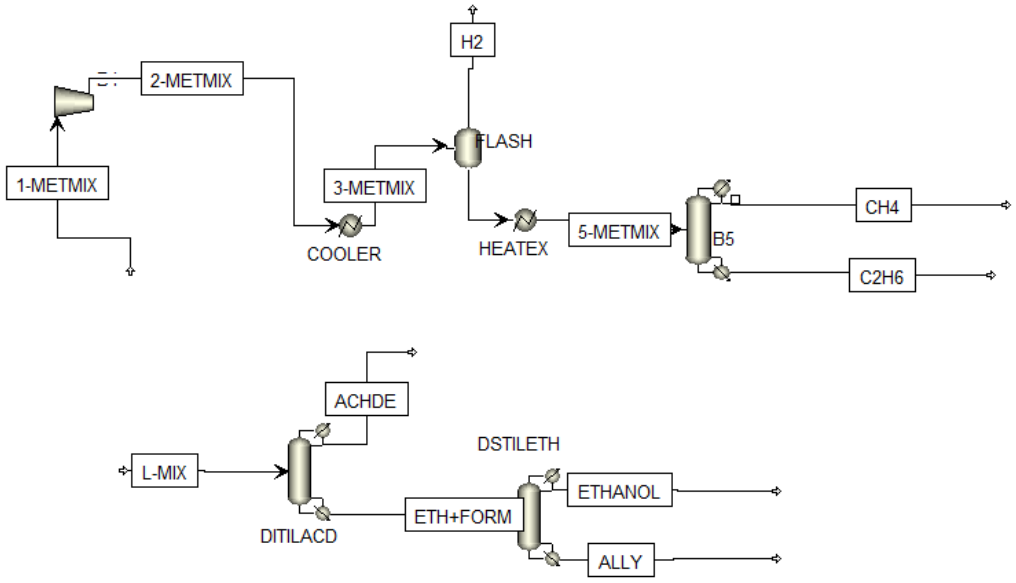

Figure 4.1: ASPEN model of the downstream separation without included extra distillation column for the ethylene purification. Similarly to the overviews shown in previous chapters, this is the working model to separate the output products in their pure form. The top installation is the gaseous stream starting at 1-METMIX and ends in the pure forms H2, CH4 and C2H6 streams. Below is the theoretical model of the liquid separation.

The ASPEN model shown in figure 4.1 is the setup used to produce the final separated pure components. From the top, in the 1-METMIX stream, the gaseous products are expelled from the electrolyser, and with the CO_2 removed. This comes in at a temperature of $25°C$ and 1 atm. From there, there is an initial compression stage increasing the pressure to 10 bar. This is done to reduce the amount of cooling required for the flash and cryogenic distillation stage. After the Compressor, the 2-METMIX stream is fed into a cooler, which lowers the temperature to $-150°C$. After which, the flash separator is used to remove the H_2.

Finally, the CH_4 and C_2H_4 stream is fed into a heater, increasing the temperature to $-50°C$ before being fed into the cryogenic distillation stage. This stage runs at $-124°C$ for the CH_4 and $-56°C$ for the C_2H_4. At these temperatures the phases are liquid. From modelling in the DTSWU a reflux ratio of 0.27 and 44 stages are used in the distillation column.

For the L-mix stream, there is a simplified model used to separate the liquid products. Due to the concentration being very low, the impact of this on the overall production costs is negligible and will therefore be negated. However, there is still a working model with the pure components separated with the use of two distillation columns.

The outputs of the model are used in the CAPEX calculations. Inputs are taken from the electrolyzer. Once the outputs are found, it can be put into the streams, and it will create an output depending on the scenario. Each of the outputs is then fed back into the cost modelling.

4.3.1 Cryogenic Flash Separation Performance

The flash separation stage of the process was analyzed to assess its ability to purify the vapour and liquid product streams from the cryogenic cooling and depressurization of the reactor effluent. Operating at a pressure of 10 bar and temperatures between $-110°C$ and $-150°C$, the system enables phase separation of the hydrocarbon and hydrogen-rich components.

The vapour stream (3-METMIX) exiting the cooler predominantly consists of light gases, with hydrogen (HYDRO-01) and methane (METHA-01) making up nearly 86% of the mass fraction, indicative of successful enrichment of volatile components. The molar vapour fraction of this stream is 1.0, confirming complete vaporization, and the low mass density further confirms the gaseous nature of the mixture.

In contrast, the liquid stream (4-METMIX) leaving the flash unit shows a strong presence of heavier hydrocarbons, with ethylene (ETHYL-01) accounting for approximately 46% of the mass and methane for around 54%. The hydrogen content in this stream is negligible, highlighting the effective phase separation achieved by the flash process. The high molar and mass densities and the complete liquid phase confirm effective condensation and separation of heavier components.

Overall, the separation results indicate high purity of the vapour and liquid phases in terms of their dominant constituents, supporting the use of cryogenic flash separation as an effective technique for upgrading the product stream prior to further purification or reuse.

4.3.2 Cryogenic Distillation

The performance of the cryogenic distillation column tasked with separating a methane-ethylene mixture was evaluated based on detailed ASPEN Plus simulation outputs. The feed stream (`5-METMIX`) consisted of a vapour-phase mixture at −50°C and 10 bar, The column successfully split this stream into two liquid-phase product streams at 15 bar: one rich in ethylene (C_2H_4) and the other in methane (CH_4).

The ethylene-rich stream (C_2H_4) contains 97.98% ethylene species by mole. This indicates it is a high-enthalpy stream that requires cooling to achieve the desired separation. The methane-rich stream (CH_4) is exceptionally pure, with 99.5% methane on a molar basis.

Overall, the column achieves high separation performance with minimal methane slip in the ethylene stream, indicating a well-optimized cryogenic design. The data support the viability of the distillation unit as an energy-intensive but high-purity purification method downstream of electrochemical CO_2 methane reduction.

4.4. ASPEN Results

4.4.1 Product Stream Performance: Methane, Ethylene and Hydrogen

The final product streams from the system, namely methane (CH_4), ethylene (C_2H_4), and hydrogen (H_2), exhibit distinct characteristics with respect to phase behavior, composition, and purity, demonstrating the effectiveness of cryogenic separation in achieving targeted component recovery.

Table 4.2: Key Parameters for Final Product Streams

Component	Mass Fraction	Mass Flow Rate (kg/h)
Methane (CH_4)	99.99%	1945.03
Ethylene (C_2H_6)	88.65%	133.67
Hydrogen (H_2)	99.82%	394.21

The methane stream is withdrawn as a compressed liquid at −124°C and 9.9 bar. The composition analysis reveals an extremely high mole fraction of 99.95% CH_4, with negligible contamination by other hydrocarbons or hydrogen. The high purity, coupled with the relatively low specific entropy and high mass density (0.36 g/cm^3), supports its suitability for direct use or liquefaction as part of synthetic natural gas (SNG) supply.

The ethylene stream is similarly recovered as a liquid from a different branch, operating at −73.76°C

and 10 bar. It contains 82.87% ethylene and 17.13% methane by mole. While not as pure as the methane or hydrogen product streams, it still represents a commercially viable composition for downstream use or further purification. The stream's relatively higher density (0.49 g/cm^3) and molar enthalpy indicate a more condensed state suitable for storage or conversion processes.

The hydrogen stream is discharged as a vapour at −150°C and 10 bar. It shows a mole fraction of 99.9% hydrogen, demonstrating excellent separation. The high purity and relatively low mass density (0.0046 g/cm^3) are characteristic of gaseous hydrogen under cryogenic conditions. The low enthalpy and entropy values further confirm the stream's suitability for compression or energy storage applications. Hydrogen generated during this process will be sold as green hydrogen. This will give a higher price and allow for the utalization of the by-products. In the end, there is a relatively large amount of hydrogen produced, and thus selling to the industry will be a vital source of income.

Improving the purity of the streams could enhance the profitability of the process. In figure 4.2, a method to enhance the purities by using an extra cryogenic distillation column with a recycle stream, which is then fed back into the 5-METMIX was included. This increases the overall output of the model.

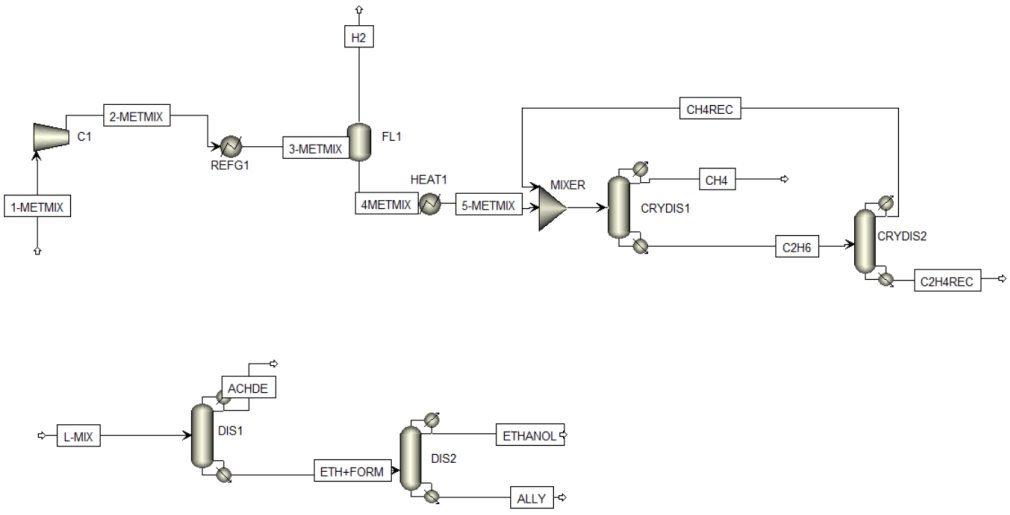

Figure 4.2: ASPEN model of the separation and increased purity of ethylene stream. By adding an additional distillation column it is possible to increase the quality of the C2H6 stream. This has benefits but increases capital, costs without a real gain in sales.

Including a recycle increases the purity of the CH_4 and C_2H_4 stream. The results of the extra distillation column are shown in table 4.3. The purity of the C_2H_4 rose to 11 %. Also, the output of the CH_4 is increased as improved recycling with subsequent capture to improve the overall effectiveness of the separation side of the process. On the other hand, higher purity does come at a cost of adding extra steps to the process and raising the power consumption.

Table 4.3: Key Parameters for Final Product Streams with recycle

Component	Mass Fraction	Mass Flow Rate (kg/h)
Methane (CH_4)	99.99%	1964.23
Ethylene (C_2H_6)	99.8%	149.40
Hydrogen (H_2)	99.82%	394.21

However, the extra cost of the cryogenic distillation column required an additional investment of 221,100

EUR, according to ASPEN. Looking at the difference in the amount produced by the design with no recycle gives a difference in output of around 11.2 kg/hr for CH_4 and 6.74 for C_2H_4. At the price used for the base analysis of 1.01 EUR/kg for methane and 1 EUR/kg of ethylene. The time to repay the investment would be approximately 11600 hours. In certain scenarios, it would be multiple years of operation which would make the investment impact overall profitability of the process.

4.4.2 Product Stream Performance: Methane, Ethylene and Hydrogen

Overall, the system effectively isolates three high-purity streams, each with distinct thermodynamic and compositional properties tailored for specific downstream use cases. The cryogenic purification setup achieves strong separation performance, imperative for meeting economic and regulatory standards in methane and hydrogen production.

4.5. Economic Analysis

By comparing the scenarios stated in the previous chapter, an analysis is made comparing the economic feasibility of this large-scale process of producing methane from CO_2 using electrolysis. Some of the fixed parameters are shown below in table 4.4. Other factors, such as the stream prices, will be varied to see what the range of feasibility is. For example, the CH_4 prices will be used as max and min to show in the best case scenario.

Table 4.4: Key Technical and Economic Assumptions

Parameter	Value
Power input	100 MW
Faradaic Efficiency (FE)	40.84%
Current density	5000 A/m^2
Cell voltage	2.5V
Conversion ratio	0.60
Electrolyzer capital cost	€9000/m^2
Interest rate	5%
Tax rate	25%
Depreciation rate	5%

4.5.1 Economic Model and Calculation Methodology

To evaluate the techno-economic feasibility of the electrochemical CO_2 reduction process to methane and byproducts, a detailed discounted cash flow (DCF) model was implemented in Excel. This financial model integrates capital expenses (CAPEX), operational costs (OPEX), depreciation, tax effects, and cash flows over the project lifetime to determine metrics such as the Net Present Value (NPV).

The process model considers primary input streams such as CO_2, H_2O, and electricity. The outputs include CH_4 as the main product, along with valuable byproducts like H_2, C_2H_4, and $HCOO^-$. These product streams are multiplied by their market prices to calculate the total annual sales revenues according to

$$Sales = \sum_i \dot{m}_i \times P_i \tag{4.1}$$

where $\dot{m}_i$ is the mass flow of product i and P_i its market price.

The total capital investment is divided between the electrolyzer section and the downstream separation unit. Additionally, a working capital cost is considered as a fraction of the total capital cost to cover initial

operational needs. The OPEX includes both fixed and variable costs, such as maintenance, electricity, and feedstock costs for CO_2 and water. Depreciation is calculated using a straight-line method over the economic lifetime, thereby reducing taxable profits.

Each year, the model determines the net profit before tax by subtracting OPEX and depreciation from the total sales revenue. Applying the income tax rate yields the income after tax (IAT). Adding back non-cash depreciation gives the operating cash flow (OCF), defined by

$$OCF = IAT + Depreciation \tag{4.2}$$

To account for the time value of money, each year's cash flow is discounted back to present value using the selected discount rate r, resulting in the discounted cash flow (DCF) for year t:

$$DCF_t = \frac{OCF_t}{(1+r)^t} \tag{4.3}$$

The Net Present Value (NPV) is then calculated by summing the discounted cash flows over the project lifetime and subtracting the initial investments, expressed as

$$NPV = -(CAPEX + WorkingCapital) + \sum_{t=1}^{N} DCF_t \tag{4.4}$$

where the upfront CAPEX and working capital are treated as an initial negative cash flow.

At the end of the project life, a salvage value is included as a fraction of the initial capital, discounted to present value. This adjustment positively contributes to the final NPV.

This comprehensive approach provides a rigorous financial assessment of the process under realistic market conditions. It allows the identification of key economic drivers, such as electricity price, CO_2 pricing, and product values, and enables sensitivity analyses to investigate how individual parameters influence economic outcomes. Through this methodology, it becomes possible to assess the competitiveness of the electrochemical CO_2 reduction process to methane under various scenarios, offering insights critical for investment decisions and policy considerations.

4.5.2 NPV Results

Below is an overview of the NPV values for the industrial process with the specified parameters. It is important to consider that the two lines are the best and worst cases within the individual scenarios. These differences are mostly due to the difference in the prices of CH_4 and H_2.

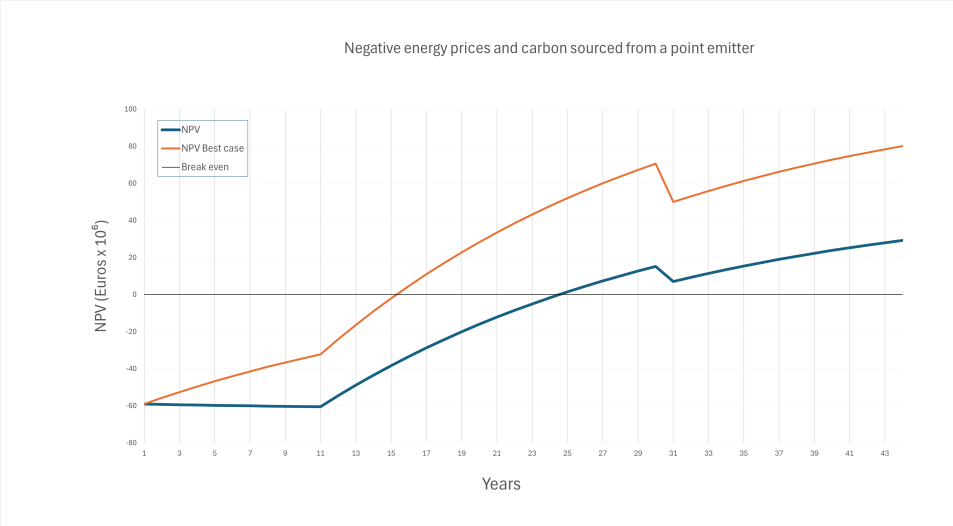

Figure 4.3: Scenario 1: Net Present Value (NPV) over 44 years. This scenario describes the best case for operation. The plant would only run during negative energy prices, which are occurring during the hours from 12 to 16:00.

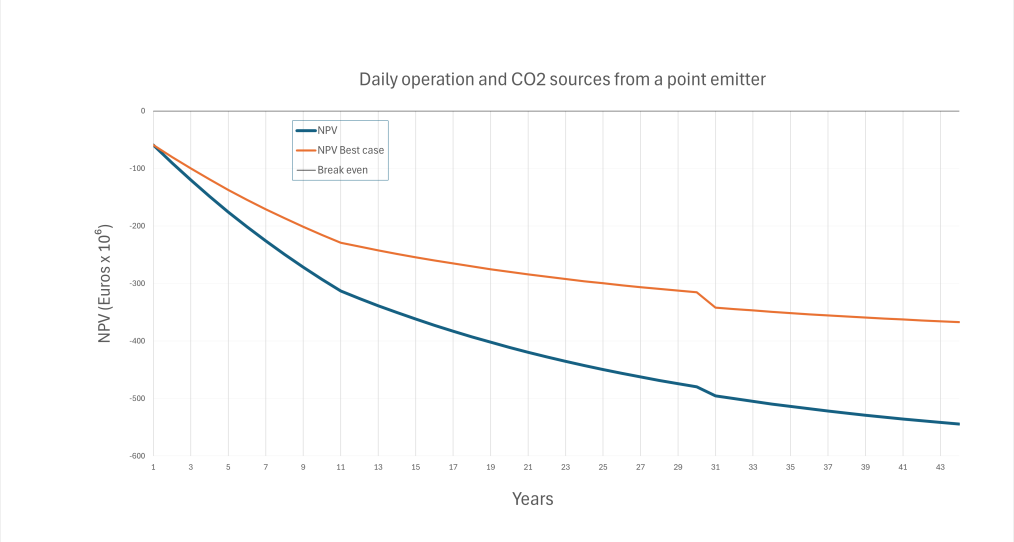

Figure 4.4: Scenario 2: NPV with daily operation and CO_2 from a point source. For this scenario, a full daily operation is taken with 24 hour operation with a total time taken of 8000 hours. This with the energy prices averaged over this time, creates a NPV that always stays negative regardless of the CH_4 and H_2 prices. For this scenario there is no profitability possible.

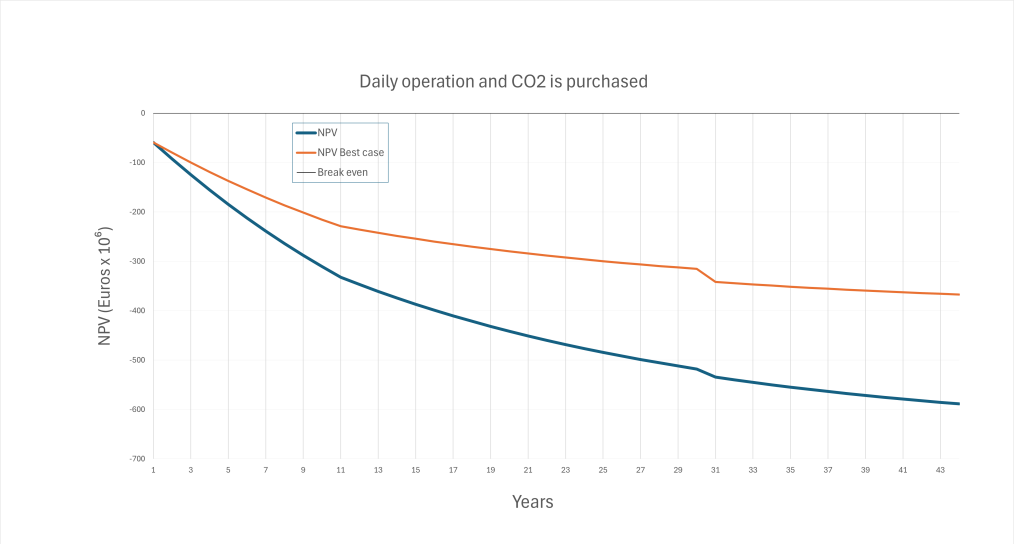

Figure 4.5: Scenario 3: NPV with daily operation and purchased CO_2. Similar to scenario 2, this graph illustrates no positive NPV. Over time, there is still more cost than income seen by the downward sloping trend. As the energy prices have a large influence on this process, unless there are negative or low energy prices it will not become feasible in the future.

Figure 4.6: Scenario 4: NPV using 2024 market prices. In this scenario, the most realistic prices for energy are taken. Almost identical to the previous scenarios 1,2, there is no profitability even with the best case for the outputs.

Using the different ranges of values, it can be seen that the energy prices will have the most effect on the NPV. This, however, is the highest price of energy in the Netherlands for energy usage and can be considered only for operation during peak hours. This still needs to be considered as it will have an effect when operating. When looking at the prices [Jouny et al. 2018b], there is variation during the operating hours prices. In this case, scenario 1 would factor in operating only when the prices do not peak and keep the plant running in a profitable zone.

Analysing the results from the model, it is seen that the first case scenario is where the plant would run only at specific moments. Using the highest and lowest price scenarios also shows that in the cases where full operation would apply, product price does not have a large enough effect. Due to the range of the energy prices -100 Eur/MWh to 280 Eur/MWh gives more of a difference compared to the CH_4 prices. The market for CH_4 being very competitive, utilizing the low costs will be imperative to create an economically viable electrolyzer. Electricity prices are, therefore, the most vital to the process. However,

it is unlikely that a plant of this scale would be able to run intermittently due to the capital costs, making it dependent on future electricity prices. Estimates have been made that the levelized cost of electricity (LCOE) will be around $ 36/MWh [Lazard 2025]. From these scenarios, it can be concluded that energy prices are critical in the operation and further analysis must be done to realise the other parameters that can result in feasible operation.

Figure 4.7: The pricing used from Lazard's estimates for renewable energy prices in the US. Prices are converted into euros as the assumption that the plant will run in the Netherlands. However, it is assumed that the pricing for renewable energies in the US and Europe will be similar.

In figure 4.7, the range presented as the best and worst case could provide in the case of future feasibility. However, the profitability would be highly dependent on the prices of the streams. Looking at the current market, it would indicate that the prospects of profitability are marginal. However, as shown in the IEA report [International Energy Agency 2025], natural gas demand is at an all-time high. Additionally, the increasing CO_2 emissions and increased pressure to capture CO_2, which could lead to lower CO_2 prices and higher CH_4 demand with the reduction of natural gas winning, could improve the possibilities. Subsequently, there will be a more hospitable market environment for this type of process.

4.5.3 Value Chain Analysis

Analysing the entire value chain of the process will indicate where the largest costs and profits are made. Furthermore, analysing the entire process from the capture of CO_2 to the purified products, including recycling and sale, allows for an in-depth discussion on the bottlenecks and requirements for this process to become feasible for the production of CH_4. Increasing volatility in the electricity market due to the overproduction from wind and solar creates opportunities and challenges for large-scale processes.

Uncertainties in the overall market and the operation's best and worst case scenarios are evaluated to understand the economics of this process. Using the ASPEN function together with the electrolyzer model with the set parameters, the CAPEX, OPEX, and sales figures will be simulated in these worst and best case scenarios. In the sensitivity analysis, the NPV at 30 years is calculated and shown as the outcome.

Table 4.5: Product price ranges used in economic analysis

Parameter	Min	Max
CH_4 Price (euro/kg)	0.791	1.41
H_2 Price (euro/kg)	9.5	11.5
$HCOO^-$ Price (euro/kg)	0.5	1.5
CO_2 Price (euro/kg)	-0.05	0.10

Table 4.6: Ranges for electrolyzer and process parameters

Parameter	Min	Max
Faradaic efficiency (%)	24.4	81.7
Cell voltage (V)	1.6	3.5
Conversion ratio (-)	0.4	0.8
Current density (A/m^2)	1000	7500
Electrolyzer cost (euro/m^2)	4000	14000
CO_2 separation cost (euro/year)	12000	32000
Low energy prices (euro/kWh)	-0.028	0.28

Table 4.6 shows the value ranges taken for the sensitivity analysis. Ranges for the prices are found in literature and on government websites. For the electrolyzer some estimates were made as some values are found experimentally and have not been tested at a larger scale. For example, the FE all have associated CD, but in this, they are varied with one staying constant to illustrate the effect that technological developments have on the economic outlook. FE are experimental and do not sustain stability close to the 8000 hours used in the analysis.

From the NPV calculations, it is unclear what is specifically causing the large discrepancy in the values. There is a large difference once the prices for CH_4 and H_2 vary from 0.791 to 1.41 and from 2 to 6, respectively. In the sensitivity analysis, various parameters are examined.

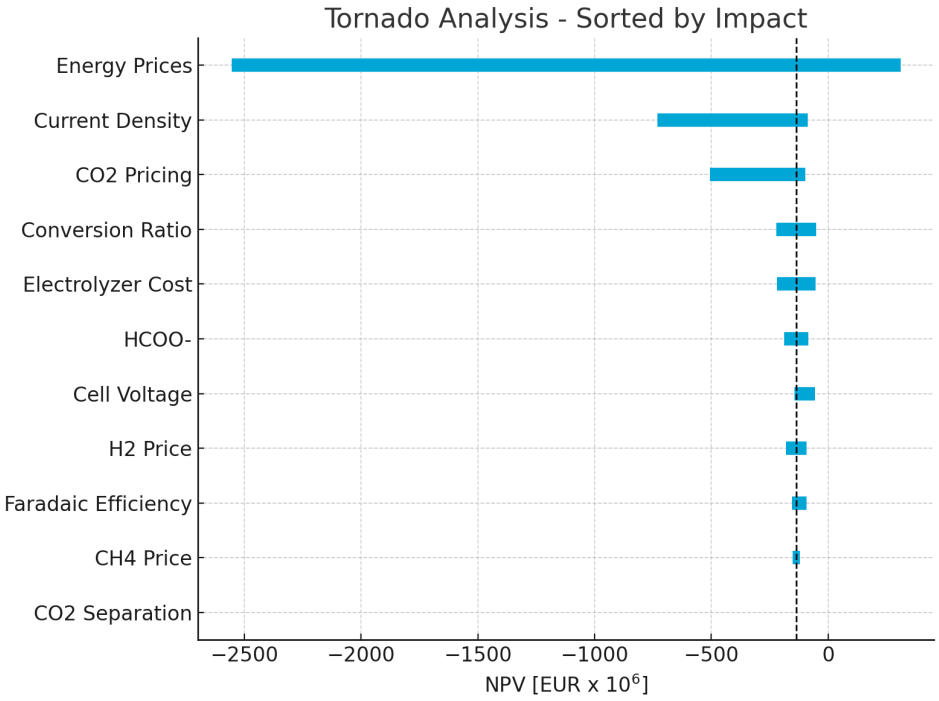

Figure 4.8: Tornado chart showing the sensitivity of NPV to different input parameters with energy prices incorporating the cooling and heating costs.

To compete with conventional fossil-based methane production, the electrochemical CO_2 to CH_4 route must meet several key conditions. Firstly, electricity prices must below €0.03–€0.04 per kWh, particularly if operating at high current densities where energy dominates operating costs. For the current market energy prices, the price of CH_4 would need to be 5.8 Eur/kg to have a positive NPV within 30 years shown in the NPV CH_4 profitability table in the appendix. However, comparing this to the natural gas price range taken as 0.781 to 1.41 Eur/kg, the price gap is large, requiring low energy prices for this process to become feasible.

The estimated ratio of OPEX to CAPEX of approximately 1:2 is based on assumptions, as there are currently no large-scale CO_2 electrolyzers in operation. By comparing different electrolyzer technologies, such as finding a midpoint between the costs of solid oxide electrolyzer cells (SOEC) and chlor-alkali electrolyzers, an approximate capital cost of around €14,000/MWh can be derived [De Gregorio et al. 2020]. Under this assumption, the OPEX to CAPEX ratio increases to roughly 1:4.

This variation arises primarily from the sizing of the electrolyzer, which depends on the current density and cell voltage. Increasing the current density allows the electrolyzer to process more power per unit area, thereby reducing the required footprint and lowering the CAPEX. However, this has minimal direct effect on the downstream separation, which is more strongly linked to the Faradaic efficiency (FE) and selectivity of the electrochemical process.

As illustrated in the tornado chart (Figure 4.8), the product stream prices significantly influence the net present value (NPV) of the process. The relatively stable price of CH_4 means its impact on the NPV is less pronounced compared to other products. Despite methane being the main target of the process, its low market price reduces its contribution to the overall revenue. In contrast, byproducts such as formate ($HCOO^-$) and hydrogen (H_2) exhibit greater sensitivity. Due to the molecular mass of formate, larger mass flows are produced than for CH_4, amplifying its economic impact. This highlights the importance of co-product valorization in achieving economic feasibility.

Downstream separation costs are estimated to contribute less than 10% to the total process cost. However, it is important to note that this figure stems from a simplified model. In reality, depending on product

purity specifications and separation technology, these costs could be considerably higher. For example, using countercurrent hollow fiber membrane models indicates that achieving higher product purities substantially increases capital costs [Pettersen and Lien 1994].

For this process to become profitable, favorable market conditions and significant technological advances in CO_2 electrolysis are necessary. Improving current density and Faradaic efficiency directly enhances electrolyzer productivity, reducing CAPEX per unit output. Additionally, increasing the CO_2 conversion ratio ensures more effective utilization of the 100 MW electrical input considered in this study, thereby improving process efficiency. Achieving higher conversion rates requires careful electrolyzer design and optimization of operational parameters.

A critical factor for long-term economic viability is the cost of electricity. Given that energy prices dominate OPEX in power-to-X processes, future reductions in renewable electricity costs are promising for improving profitability. Furthermore, the classification of the produced hydrogen as "green hydrogen" is contingent on using renewable electricity sources, which is essential for capturing potential premium pricing or meeting regulatory standards. It should also be noted that downstream purification, especially for hydrogen, plays a pivotal role. While this study assumes simplified separations, actual processes must consider purity targets that can significantly influence both capital and operating expenditures. As indicated by membrane modeling studies, pushing to higher purities drives up investment costs.

In conclusion, a combination of improved electrolyzer performance (through higher current densities, efficiencies, and conversion ratios), lower energy costs, and strategic co-product utilization is essential to establish an economically viable large-scale CO_2 electroreduction process. Future work should also investigate advanced integration strategies with existing industrial infrastructure to leverage shared utilities and reduce overall costs.

5

Discussion and Conclusion

During the literature review, there were clear indications that an industrial-scale CO_2 electrolyzer would be a challenge. Factors that hinder the application of the CO_2RR technology are stability, selectivity, costs and investments, CO_2 sources, and the demand for methane. In this chapter, the results will be used to analyze the real-world application and feasibility.

5.1. Overview

This study has modelled and evaluated the electrochemical reduction of CO_2 to CH_4 at industrial scale, assessing both technical and economic feasibility. The results indicate that while production of high-purity methane through CO_2RR is technically achievable with demonstrated Faradaic efficiencies (FE) near 41% and high-purity output streams, the pathway remains economically marginal under current market conditions without favourable pricing scenarios or subsidies. To examine these findings, this discussion compares the modelling results with advancements and challenges identified in the literature.

5.2. Efficiency and Catalyst Limitations

The modelled system operates with a Faradaic Efficiency of 40.84% and a cell voltage of 2.5 V at a current density of 5000 A/m^2. While these values demonstrate strong progress toward industrial-scale operation, literature confirms that such performance benchmarks remain at the edge of current capabilities. For instance, most CH_4-selective systems operate below 3000 A/m^2 with FEs for CH_4 typically ranging from 24% to 55% Zhang et al. 2023].

During the electrolysis, it is challenging to achieve the desired high current densities, Faradaic efficiencies, and overall efficiencies, particularly for methane, which remains among the most energy-intensive CO_2RR products due to the 8-electron transfer required. Cases in the model are taken as the most optimal case.

Cu-based catalysts, while uniquely capable of producing hydrocarbons like CH_4 and C_2H_4, suffer from serious degradation mechanisms such as fragmentation, reshaping, and agglomeration, limiting long-term operation. A proposed asymmetric low-frequency pulsed strategy (ALPS) achieved CH_4 selectivity >80% for over 300 hours, which is a major leap forward. However, such performance has yet to be translated to standard, continuous industrial settings [Jin et al. 2021]. In this case, less energy would be needed for the separation of the gaseous products.

5.3. Stability and Durability of the Electrolyzer

One of the most prominent findings of the techno-economic model is the critical role that electrolyzer lifetime and durability play in determining feasibility. In the modelled system, component degradation was not explicitly simulated, but literature suggests this is a dominant bottleneck [Engelbrecht and Bessarabov 2018].

Most systems today are limited to operation times below 100 hours, far short of the 80,000 hours seen in commercial alkaline water electrolysis. Operating the electrodes for (>1000 h) in these systems is a key issue in the production [Engelbrecht and Bessarabov 2018], and long-term degradation, particularly of Cu catalysts, poses a critical challenge to scale-up.

5.4. Energetic and Economic Constraints

While this process demonstrates high product purity and effective cryogenic separation of CH_4, H_2, and C_2H_4, the energy consumption remains high. Energetic efficiency, calculated to be 63%, is constrained by overpotentials and large voltage requirements.

From the economic perspective, the thesis shows that CH_4 prices must exceed €1.41/kg and energy prices remain low (≈€0.025/kWh) for profitability within a 5-year timeframe. These results differ from the analysis of Jouny et al., who found that methane is not profitable under current market conditions, with NPVs for CH_4 remaining negative even under optimistic assumptions. This is due to the various low to negative energy prices. In these cases, the production could become profitable. However, this would reduce the operation window and reduce overall profits.

5.5. Separation and System Integration

The ASPEN model's cryogenic separation demonstrates that gas-phase CH_4 can be isolated at 99.95% purity, which is commercially valuable. However, such purity comes at the cost of energy-intensive refrigeration, contributing to operational expenses.

Moreover, unreacted CO_2 is recycled, which improves overall conversion efficiency but introduces complexity in system integration, including flow balancing and pressurization. These dynamics must be optimized further to reduce parasitic losses and improve net energy yield. Taking into account the CO_2 separating from the stream, an energy penalty must be added.

5.6. Outlook and Future Considerations

Catalyst degradation remains a major limitation for CO_2 reduction to methane, with Cu-based systems suffering from morphology changes and shifts in oxidation state that reduce long-term activity. Electrolyte optimization and improved membrane design are key to minimizing HER and enhancing CH_4 selectivity. There still needs to be consideration of the costs of the process. At the system level, incorporating energy recovery, heat integration, and flexible operation aligned with renewable energy availability can improve efficiency and economics. Finally, due to methane's low market value, robust policy incentives and CO_2 credit schemes will be critical to render these processes commercially viable.

5.7. Conclusion

This discussion demonstrates that while the modelled system is technically feasible with performance and separation consistent with current literature, the challenges in durability, selectivity, energetic efficiency, and market economics significantly restrict deployment at scale. Improvements in stable catalysts, system design, and process intensification, as well as policy frameworks that value carbon removal, will be pivotal in making CO_2RR to CH_4 a competitive and climate-aligned technology.

The running of the plant is only possible with low prices for energy and high prices for CH_4. The future depends heavily on the government's intervention in subsidising the CO_2 to allow for low costs. Reaching the Net-zero goals by 2050 and reducing the anthropogenic release of greenhouse gases, whilst also utilising the captured gases, will play a vital role in the coming years. Subsequently, producing carbon molecules from captured CO_2 will open a new chapter in the possible incentivising of companies to change their current processes, and introduce carbon capture technologies.

Bibliography

Abdullatif, Y., Sodiq, A., Mir, N., Bicer, Y., Al-Ansari, T., El-Naas, M. H., and Amhamed, A. I. (2023). Emerging trends in direct air capture of co_2: a review of technology options targeting net-zero emissions. *RSC Advances*, 13(9):5687–5722.

Babacan, O., De Causmaecker, S., Gambhir, A., Fajardy, M., Rutherford, A. W., Fantuzzi, A., and Nelson, J. (2020). Assessing the feasibility of carbon dioxide mitigation options in terms of energy usage. *Nature Energy*, 5(9):720–728.

Blanco, H., Nijs, W., Ruf, J., and Faaij, A. (2018). Potential of power-to-methane in the eu energy transition to a low carbon system using cost optimization. *Applied Energy*, 232:323–340.

Cai, Y., Fu, J., Zhou, Y., Chang, Y.-C., Min, Q., Zhu, J.-J., Lin, Y., and Zhu, W. (2021). Insights on forming n,o-coordinated cu single-atom catalysts for electrochemical reduction of co to methane. *Nature Communications*, 12(1):1288. https://doi.org/10.1038/s41467-020-20769-x.

Cave, E. R., Montoya, J. H., Shi, C., Hatsukade, T., Abram, D. N., Kuhl, K. P., and Jaramillo, T. F. (2018). Electrochemical co_2 reduction on nanostructured cu: Selecting products through morphology tuning. *Catalysis Today*, 288:78–85.

Costentin, C., Robert, M., and Savéant, J. M. (2013). Catalysis of the electrochemical reduction of carbon dioxide. *Chemical Society Reviews*, 42(6):2423–2436.

De Gregorio, G. L., Burdyny, T., Loiudice, A., Iyengar, P., Smith, W. A., and Buonsanti, R. (2020). Electroreduction of co_2/co to c_2 products: Process modeling, downstream separation, system integration, and economic analysis. *ACS Sustainable Chemistry & Engineering*, 8(22):8316–8328. https://doi.org/10.1021/acssuschemeng.0c01738.

De Jesús-Cardona, H., Del Moral, C., and Cabrera, C. R. (2001). Voltammetric study of co_2 reduction at cu electrodes under different $khco_3$ concentrations, temperatures, and co_2 pressures. *Journal of Electroanalytical Chemistry*, 513(1):45–51. https://doi.org/10.1016/S0022-0728(01)00572-2.

Delacourt, C., Ridgway, P. L., Kerr, J. B., and Newman, J. (2008). Design of an electrochemical cell making syngas (co + h_2) from co_2 and h_2o reduction at room temperature. *Journal of Electrochemical Society*, 155(1):B42–B49. https://doi.org/10.1149/1.2801871.

Durand, W. J., Peterson, A. A., Studt, F., Abild-Pedersen, F., and Nørskov, J. K. (2011). Structure effects on the energetics of the electrochemical reduction of co_2 by copper surfaces. *Surface Science*, 605(15–16):1354–1359.

Engelbrecht, J. and Bessarabov, D. (2018). Techno-economic evaluation of pem water electrolysis for hydrogen production. *Journal of The Electrochemical Society*, 165(16):J3059–J3070. https://doi.org/10.1149/2.0031816jes.

EPEX SPOT (2025). European power exchange. `https://www.epexspot.com/en`. Accessed: 2025-06-27.

Fu, D. and Davis, M. (2023). Toward the feasible direct air capture of carbon dioxide with molecular sieves by water management. *Cell Reports Physical Science*. https://doi.org/10.1016/j.xcrp.2023.101389.

Götz, M., Lefebvre, J., Mörs, F., Koch, A. M., Graf, F., Bajohr, S., Reimert, R., and Kolb, T. (2016). Renewable power-to-gas: A technological and economic review. *Renewable Energy*, 85:1371–1390.

Harris, Z., Milner, S., and Taylor, G. (2018). Biogenic carbon—capture and sequestration. pages 55–76. https://doi.org/10.1016/B978-0-08-101036-5.00005-7.

Hauch, A., Küngas, R., Blennow, P., Hansen, A. B., Hansen, J. B., Mathiesen, B. V., and Mogensen, M. B. (2020). Recent advances in solid oxide cell technology for electrolysis. *Science*, 370(6513):eaba6118.

Hori, Y. (2008). Electrochemical co_2 reduction on metal electrodes. In Conway, B. E., White, R. E., and Bockris, J. O., editors, *Modern Aspects of Electrochemistry*, volume 42, pages 89–189. Springer. https://doi.org/10.1007/978-0-387-49489-0_3.

Hori, Y., Murata, A., and Takahashi, R. (1989). Formation of hydrocarbons in the electrochemical reduction of carbon dioxide at a copper electrode in aqueous solution. *Journal of the Chemical Society, Faraday Transactions 1: Physical Chemistry in Condensed Phases*, 85(8):2309–2326. https://doi.org/10.1039/F19898502309.

Hung, S. F. (2020). Electrochemical flow systems enable renewable energy industrial chain of co_2 reduction. *Pure and Applied Chemistry*, 92(12):1937–1951.

International Energy Agency (2025). Global energy review 2025. `https://iea.blob.core.windows.net/assets/5b169aa1-bc88-4c96-b828-aaa50406ba80/GlobalEnergyReview2025.pdf`. Accessed: 2025-07-23.

Jang, J., Kim, C., Back, S., Kim, H., Kim, Y. H., and Jung, Y. (2021). Operando study of the dynamic behavior of cu surfaces during electrochemical co_2 reduction. *Energy & Environmental Science*, 14(1):200–209.

Jiang, L., Liu, W., Wang, R., González-Díaz, A., Rojas-Michaga, M., Michailos, S., Pourkashanian, M., Zhang, X., and Font-Palma, C. (2023). Sorption direct air capture with co_2 utilization. *Progress in Energy and Combustion Science*. https://doi.org/10.1016/j.pecs.2022.101069.

Jin, S., Ren, P., Zheng, Y., and Chen, J. G. (2021). Advances and challenges for the electrochemical reduction of co_2 to co: From fundamentals to industrialization. *Angewandte Chemie International Edition*, 60(24):13156–13180. https://doi.org/10.1002/anie.202013398.

Jouny, M., Luc, W., and Jiao, F. (2018a). General techno-economic analysis of co_2 electrolysis systems. *Industrial & Engineering Chemistry Research*, 57(6):2165–2177. https://doi.org/10.1021/acs.iecr.7b03514.

Jouny, M., Luc, W., and Jiao, F. (2018b). General techno-economic analysis of co_2 electrolysis systems. *Industrial & Engineering Chemistry Research*, 57(6):2165–2177. https://doi.org/10.1021/acs.iecr.7b03514.

Kimura, K. W., Fritz, K. E., Kim, J., Suntivich, J., Abruña, H. D., and Hanrath, T. (2018). Controlled selectivity of co_2 reduction on copper by pulsing the electrochemical potential. *ChemSusChem*, 11(11):1781–1786.

Kortlever, R., Shen, J., Schouten, K. J. P., Calle-Vallejo, F., and Koper, M. T. M. (2015). Catalysts and reaction pathways for the electrochemical reduction of carbon dioxide. *Journal of Physical Chemistry Letters*, 6(20):4073–4082.

Lazard, I. (2025). Levelized cost of energy (lcoe) — 18th edition. `https://www.lazard.com/research-insights/levelized-cost-of-energyplus-lcoeplus/`. PDF report; annual analysis of energy generation, storage, and hydrogen costs.

Lim, R. J., Xie, M., Sk, M. A., Lee, J. M., Fisher, A., Wang, X., and Lim, K. H. (2014). A review on the electrochemical reduction of co_2 in fuel cells, metal electrodes and molecular catalysts. *Catalysis Today*, 233:169–180.

Liu, P. X., Peng, L. W., He, R. N., Li, L. L., and Qiao, J. L. (2022). A high-performance continuous-flow mea reactor for electroreduction co_2 to formate. *Journal of Electrochemistry*, 28(1):3.

Luyben, W. L. (2017). Estimating refrigeration costs at cryogenic temperatures. *Computers & Chemical Engineering*, 103:144–150.

Merino-Garcia, I., Alvarez-Guerra, E., Albo, J., and Irabien, A. (2016). Electrochemical membrane reactors for the utilisation of carbon dioxide. *Chemical Engineering Journal*, 305:104–120.

Möller, T. et al. (2023). Electrochemical co_2 reduction to methane at high current density with selectivity over 80%. *Nature Communications*, 14.

Paltsev, S., Jacoby, H. D., Reilly, J. M., Ejaz, Q. J., Morris, J., O'Sullivan, F., and Kragha, O. (2011). The future of us natural gas production, use, and trade. *Energy Policy*, 39(9):5309–5321.

Pangan, M. and Mulder, M. (2017). Influence of environmental policy and market forces on coal-fired power plants: Evidence on the dutch market over 2006–2014. Technical report, SOM Research Reports.

Park, S., Wijaya, D. T., Na, J., and Lee, C. W. (2021). Towards the large-scale electrochemical reduction of carbon dioxide. *Catalysts*, 11(2):253.

Peters, L., Hussain, A., Follmann, M., Melin, T., and Hägg, M. B. (2011). Co_2 removal from natural gas by employing amine absorption and membrane technology—a technical and economical analysis. *Chemical Engineering Journal*, 172(2-3):952–960.

Peterson, A. A., Abild-Pedersen, F., Studt, F., Rossmeisl, J., and Nørskov, J. K. (2010). How copper catalyzes the electroreduction of carbon dioxide into hydrocarbon fuels. *Energy & Environmental Science*, 3(10):1311–1315. https://doi.org/10.1039/c0ee00071j.

Pettersen, T. and Lien, K. (1994). A new robust design model for gas separating membrane modules, based on analogy with counter-current heat exchangers. *Computers & Chemical Engineering*, 18:427–439.

Rendón-Calle, A., Builes, S., and Calle-Vallejo, F. (2018). A brief review of the computational modeling of co_2 electroreduction on cu electrodes. *Current Opinion in Electrochemistry*. https://doi.org/10.1016/j.coelec.2018.03.012.

Santos, B., Khatiwada, D., and Vasudevan, R. (2022). Decarbonization of natural gas systems in the eu – costs, barriers, and constraints of hydrogen production with a case study in portugal. *Renewable and Sustainable Energy Reviews*. https://doi.org/10.1016/j.rser.2022.112775.

Singh, H., Li, C., Cheng, P., Wang, X., and Liu, Q. (2022). A critical review of technologies, costs, and projects for production of carbon-neutral liquid e-fuels from hydrogen and captured co_2. *Energy Advances*, 1(9):580–605.

Sánchez, O. G., Birdja, Y. Y., Bulut, M., Vaes, J., Breugelmans, T., and Pant, D. (2019). Recent advances in industrial co_2 electroreduction. *Current Opinion in Green and Sustainable Chemistry*, 16:47–56.

Tang, W., Peterson, A. A., Varela, A. S., Jovanov, Z. P., Bech, L., Durand, W. J., and Nørskov, J. K. (2012). The importance of surface morphology in controlling the selectivity of polycrystalline copper for co_2 electroreduction. *Physical Chemistry Chemical Physics*, 14(1):76–81.

Terlouw, T., Treyer, K., Bauer, C., and Mazzotti, M. (2021). Life cycle assessment of direct air carbon capture and storage with low-carbon energy sources. *Environmental Science & Technology*, 55(16):11397–11411.

Theo, W., Lim, J., Hashim, H., Mustaffa, A., and Ho, W. (2016). Review of pre-combustion capture and ionic liquid in carbon capture and storage. *Applied Energy*, 183:1633–1663. https://doi.org/10.1016/j.apenergy.2016.09.103.

Trading Economics (2025). Eu natural gas. `https://tradingeconomics.com/commodity/eu-natural-gas`. Accessed: 2025-06-27.

van der Giesen, C., Meinrenken, C. J., Kleijn, R., Sprecher, B., Lackner, K. S., and Kramer, G. J. (2017). A life cycle assessment case study of coal-fired electricity generation with humidity swing direct air capture of co_2 versus mea-based postcombustion capture. *Environmental Science & Technology*, 51(2):1024–1034.

Verma, S., Kim, B., Jhong, H. R. M., Ma, S., and Kenis, P. J. (2016). A gross-margin model for defining technoeconomic benchmarks in the electroreduction of co_2. *ChemSusChem*, 9(15):1972–1979.

Wang, X., Xu, A., Li, F., Hung, S.-F., Nam, D.-H., Gabardo, C. M., Wang, Z., Xu, Y., Ozden, A., Rasouli, A. S., Ip, A. H., Sinton, D., and Sargent, E. H. (2020). Efficient methane electrosynthesis enabled by tuning local co availability. *Journal of the American Chemical Society*, 142(28):14668–14673. https://doi.org/10.1021/jacs.9b12445.

Whipple, D. T. and Kenis, P. J. (2010). Prospects of co_2 utilization via direct heterogeneous electrochemical reduction. *Journal of Physical Chemistry Letters*, 1(24):3451–3458.

Wilberforce, T., Baroutaji, A., Soudan, B., Al-Alami, A. H., and Olabi, A. G. (2019). Outlook of carbon capture technology and challenges. *Science of the Total Environment*, 657:56–72.

Xie, J., Huang, Y., Wu, M., and Wang, Y. (2019). Electrochemical carbon dioxide splitting. *ChemElectroChem*, 6(6):1587–1604.

Yang, H., Hu, Y., Chen, J., Balogun, M., Fang, P., Zhang, S., Chen, J., and Tong, Y. (2019). Intermediates adsorption engineering of co_2 electroreduction reaction in highly selective heterostructure cu-based electrocatalysts for co production. *Advanced Energy Materials*, 9. https://doi.org/10.1002/aenm.201901396.

Yin, Z., Peng, H., Wei, X., Zhou, H., Gong, J., Huai, M., and Zhuang, L. (2019). An alkaline polymer electrolyte co_2 electrolyzer operated with pure water. *Energy & Environmental Science*, 12(8):2455–2462.

Zhang, B., Zhang, J., An, P., Su, Z., Wan, Q., Tan, X., and Zheng, L. (2021). Steering co_2 electroreduction toward methane or ethylene production. *Nano Energy*, 88:106239. https://doi.org/10.1016/j.nanoen.2021.106239.

Zhang, L., Hu, S., Zhu, X., and Yang, W. (2017). Electrochemical reduction of co_2 in solid oxide electrolysis cells. *Journal of Energy Chemistry*, 26(4):593–601.

Zhang, T., Verma, S., Kim, S., Fister, T., Kenis, P., and Gewirth, A. (2020). Highly dispersed, single-site copper catalysts for the electroreduction of co_2 to methane. *Journal of Electroanalytical Chemistry*.

Zhang, Y., Chen, Q., Lin, Z., Chen, F., Wang, Q., Qiao, Y., Zhao, X., Li, Y., and Qiu, M. (2023). Asymmetric low-frequency pulsed strategy enables ultralong co_2 reduction stability and controllable c_2/c_1 selectivity. *Chemical Science*, 14:5210–5220. https://doi.org/10.1039/D2SC07189A.

Zhao, C., Dai, X., Yao, T., Chen, W., Wang, X., Wang, J., Yang, J., Wei, S., Wu, Y., and Li, Y. (2017). Ionic exchange of metal-organic frameworks to access single nickel sites for efficient electroreduction of co_2. *Journal of the American Chemical Society*, 139(24):8078–8081. https://doi.org/10.1021/jacs.7b02736.

Appendix

Energy Cooling Price overview

Table 5.1: Refrigeration Costs at Cryogenic Temperatures (adapted from Luyben, 2017)

Temperature (°C)	Refrigerant(s)	Stages	Compressor Power (MW)	Capital Cost (M$)	Annual Energy Cost (M$/yr)	TAC (M$/yr)	Cost ($/GJ)
-25	NH_3	1	0.714	1.94	0.378	0.585	18.5
-25	C_3H_6	1	1.038	1.94	0.550	0.757	24.0
-50	C_3H_6	1	1.911	3.38	1.013	1.363	43.2
-75	C_2H_4/C_3H_6	2	1.698	3.99	0.900	1.318	41.8
-100	C_2H_4/C_3H_6	2	2.365	4.09	1.253	1.686	53.5
-125	$CH_4/C_2H_4/C_3H_6$	3	3.707	6.97	1.966	2.710	85.9
-150	$CH_4/C_2H_4/C_3H_6$	3	6.256	8.84	3.315	4.250	135
-175	$N_2/CH_4/C_2H_4/C_3H_6$	4	16.02	16.29	6.369	8.090	256
-190	$N_2/CH_4/C_2H_4/C_3H_6$	4	17.07	21.89	9.043	11.35	360

Table 5.2: Main electrolysis parameters and energy requirements

Current density (A/m^2)	**Cell Voltage** (V)	**Faradaic Eff.** (%)	**Reaction**	**e^-**	**Energy** (J/mol)
1000	1.65	55.19	$CO_2 + 8H^+ + 8e^- \rightarrow CH_4 + 2H_2O$	8	1,157,820
2500	1.65	48.00	Energy for CH_4 (1 kg)	–	72,363,750
5000	1.65	40.84	$2H_2O \rightarrow O_2 + 4H^+ + 4e^-$	4	474,706
7500	1.65	24.14	Energy for 2 moles O_2	–	949,412
1120	–	56.00	–	–	–

Table 5.3: Main electrolysis data: current density, cell performance, and energy requirements.

Table 5.4: Stream prices used in economic analysis

Component	Price	Unit
CH_4	0.25	€/kg
H_2	11	€/kg
C_2H_4	1	€/kg
$HCOO^-$	0.95	€/kg
CO_2	0.20	€/kg
H_2O	1	€/m^3

Table 5.5: Key Economic Assumptions for CO_2 Electrolysis Process

Parameter	Value
Energy price	€0.08 / kWh
Conversion ratio (CO_2 to CH_4)	0.8
Operating hours per year	8000 h
Cost of electrolyzer	€9,000 / m^2
CH_4 selling price	€4 / kg
H_2 selling price	€9.5 / kg
C_2H_4 selling price	€1 / kg
$HCOO^-$ selling price	€1.5 / kg
CO_2 feed cost	€0.1 / kg
Water cost	€1 / m^3

Negative energy prices and carbon sourced from a point emitter

Table 5.6: Detailed cash flow results of the process over 44 years

Year	Capital Expenses	Working Capital	Depreciation	Net Profit	IAT	OCF	DCF	NPV
0	251,116,071	12,555,804	-	-	-	-263,671,875	-263,671,875	-263,671,875
1	-	-	26,506,696	53,325,396	20,114,025	-6,392,671	-6,088,258	-269,760,134
2	-	-	26,506,696	53,325,396	20,114,025	-6,392,671	-5,798,341	-275,558,475
3	-	-	26,506,696	53,325,396	20,114,025	-6,392,671	-5,522,230	-281,080,705
4	-	-	26,506,696	53,325,396	20,114,025	-6,392,671	-5,259,267	-286,339,971
5	-	-	26,506,696	53,325,396	20,114,025	-6,392,671	-5,008,825	-291,348,797
6	-	-	26,506,696	53,325,396	20,114,025	-6,392,671	-4,770,310	-296,119,107
7	-	-	26,506,696	53,325,396	20,114,025	-6,392,671	-4,543,152	-300,662,259
8	-	-	26,506,696	53,325,396	20,114,025	-6,392,671	-4,326,812	-304,989,070
9	-	-	26,506,696	53,325,396	20,114,025	-6,392,671	-4,120,773	-309,109,843
10	-	-	26,506,696	53,325,396	20,114,025	-6,392,671	-3,924,546	-313,034,389
11	-	-	-	53,325,396	39,994,047	39,994,047	23,383,691	-289,650,698
12	-	-	-	53,325,396	39,994,047	39,994,047	22,270,182	-267,380,516
13	-	-	-	53,325,396	39,994,047	39,994,047	21,209,697	-246,170,819
14	-	-	-	53,325,396	39,994,047	39,994,047	20,199,712	-225,971,107
15	-	-	-	53,325,396	39,994,047	39,994,047	19,237,821	-206,733,286
16	-	-	-	53,325,396	39,994,047	39,994,047	18,321,734	-188,411,552
17	-	-	-	53,325,396	39,994,047	39,994,047	17,449,270	-170,962,282
18	-	-	-	53,325,396	39,994,047	39,994,047	16,618,353	-154,343,929
19	-	-	-	53,325,396	39,994,047	39,994,047	15,827,003	-138,516,927
20	-	-	-	53,325,396	39,994,047	39,994,047	15,073,336	-123,443,591
21	-	-	-	53,325,396	39,994,047	39,994,047	14,355,558	-109,088,033
22	-	-	-	53,325,396	39,994,047	39,994,047	13,671,960	-95,416,073
23	-	-	-	53,325,396	39,994,047	39,994,047	13,020,914	-82,395,159
24	-	-	-	53,325,396	39,994,047	39,994,047	12,400,871	-69,994,288
25	-	-	-	53,325,396	39,994,047	39,994,047	11,810,353	-58,183,935
26	-	-	-	53,325,396	39,994,047	39,994,047	11,247,955	-46,935,980
27	-	-	-	53,325,396	39,994,047	39,994,047	10,712,338	-36,223,641
28	-	-	-	53,325,396	39,994,047	39,994,047	10,202,227	-26,021,414
29	-	-	-	53,325,396	39,994,047	39,994,047	9,716,407	-16,305,008
30	-	-	108,028,851	53,325,396	-41,027,591	-149,056,441	-34,488,299	-50,793,307
31	-	-	-	53,325,396	39,994,047	39,994,047	8,813,067	-41,980,239
32	-	-	-	53,325,396	39,994,047	39,994,047	8,393,397	-33,586,842
33	-	-	-	53,325,396	39,994,047	39,994,047	7,993,712	-25,593,130
34	-	-	-	53,325,396	39,994,047	39,994,047	7,613,059	-17,980,071
35	-	-	-	53,325,396	39,994,047	39,994,047	7,250,532	-10,729,539
36	-	-	-	53,325,396	39,994,047	39,994,047	6,905,269	-3,824,270
37	-	-	-	53,325,396	39,994,047	39,994,047	6,576,446	2,752,176
38	-	-	-	53,325,396	39,994,047	39,994,047	6,263,282	9,015,459
39	-	-	-	53,325,396	39,994,047	39,994,047	5,965,031	14,980,489
40	-	-	-	53,325,396	39,994,047	39,994,047	5,680,982	20,661,471
41	-	-	-	53,325,396	39,994,047	39,994,047	5,410,459	26,071,930
42	-	-	-	53,325,396	39,994,047	39,994,047	5,152,818	31,224,748
43	-	-	-	53,325,396	39,994,047	39,994,047	4,907,446	36,132,194

Daily operation and CO2 sources from a point emitter

Table 5.7: Detailed cash flow overview for the project over 44 years

Year	Capital Expenses	Working Capital	Depreciation	Net Profit	IAT	OCF	DCF	NPV
0	251,116,071	12,555,804	-	-	-	-263,671,875	-263,671,875	-263,671,875
1	-	-	26,506,696	-37,477,999	-47,988,521	-74,495,218	-70,947,827	-334,619,702
2	-	-	26,506,696	-37,477,999	-47,988,521	-74,495,218	-67,569,359	-402,189,060
3	-	-	26,506,696	-37,477,999	-47,988,521	-74,495,218	-64,351,770	-466,540,830
4	-	-	26,506,696	-37,477,999	-47,988,521	-74,495,218	-61,287,400	-527,828,231
5	-	-	26,506,696	-37,477,999	-47,988,521	-74,495,218	-58,368,953	-586,197,183
6	-	-	26,506,696	-37,477,999	-47,988,521	-74,495,218	-55,589,479	-641,786,662
7	-	-	26,506,696	-37,477,999	-47,988,521	-74,495,218	-52,942,361	-694,729,022
8	-	-	26,506,696	-37,477,999	-47,988,521	-74,495,218	-50,421,296	-745,150,318
9	-	-	26,506,696	-37,477,999	-47,988,521	-74,495,218	-48,020,282	-793,170,600
10	-	-	26,506,696	-37,477,999	-47,988,521	-74,495,218	-45,733,602	-838,904,201
11	-	-	-	-37,477,999	-28,108,499	-28,108,499	-16,434,457	-855,338,659
12	-	-	-	-37,477,999	-28,108,499	-28,108,499	-15,651,864	-870,990,523
13	-	-	-	-37,477,999	-28,108,499	-28,108,499	-14,906,537	-885,897,060
14	-	-	-	-37,477,999	-28,108,499	-28,108,499	-14,196,702	-900,093,762
15	-	-	-	-37,477,999	-28,108,499	-28,108,499	-13,520,669	-913,614,431
16	-	-	-	-37,477,999	-28,108,499	-28,108,499	-12,876,827	-926,491,258
17	-	-	-	-37,477,999	-28,108,499	-28,108,499	-12,263,645	-938,754,903
18	-	-	-	-37,477,999	-28,108,499	-28,108,499	-11,679,662	-950,434,565
19	-	-	-	-37,477,999	-28,108,499	-28,108,499	-11,123,488	-961,558,053
20	-	-	-	-37,477,999	-28,108,499	-28,108,499	-10,593,798	-972,151,851
21	-	-	-	-37,477,999	-28,108,499	-28,108,499	-10,089,331	-982,241,182
22	-	-	-	-37,477,999	-28,108,499	-28,108,499	-9,608,887	-991,850,069
23	-	-	-	-37,477,999	-28,108,499	-28,108,499	-9,151,321	-1,001,001,389
24	-	-	-	-37,477,999	-28,108,499	-28,108,499	-8,715,544	-1,009,716,933
25	-	-	-	-37,477,999	-28,108,499	-28,108,499	-8,300,518	-1,018,017,451
26	-	-	-	-37,477,999	-28,108,499	-28,108,499	-7,905,255	-1,025,922,706
27	-	-	-	-37,477,999	-28,108,499	-28,108,499	-7,528,814	-1,033,451,520
28	-	-	-	-37,477,999	-28,108,499	-28,108,499	-7,170,299	-1,040,621,819
29	-	-	-	-37,477,999	-28,108,499	-28,108,499	-6,828,856	-1,047,450,676
30	-	-	108,028,851	-37,477,999	-109,130,137	-217,158,988	-50,245,693	-1,097,696,368
31	-	-	-	-37,477,999	-28,108,499	-28,108,499	-6,193,974	-1,103,890,342
32	-	-	-	-37,477,999	-28,108,499	-28,108,499	-5,899,023	-1,109,789,365
33	-	-	-	-37,477,999	-28,108,499	-28,108,499	-5,618,118	-1,115,407,482
34	-	-	-	-37,477,999	-28,108,499	-28,108,499	-5,350,588	-1,120,758,070
35	-	-	-	-37,477,999	-28,108,499	-28,108,499	-5,095,798	-1,125,853,868
36	-	-	-	-37,477,999	-28,108,499	-28,108,499	-4,853,141	-1,130,707,009
37	-	-	-	-37,477,999	-28,108,499	-28,108,499	-4,622,039	-1,135,329,047
38	-	-	-	-37,477,999	-28,108,499	-28,108,499	-4,401,942	-1,139,730,989
39	-	-	-	-37,477,999	-28,108,499	-28,108,499	-4,192,325	-1,143,923,315
40	-	-	-	-37,477,999	-28,108,499	-28,108,499	-3,992,691	-1,147,916,007
41	-	-	-	-37,477,999	-28,108,499	-28,108,499	-3,802,563	-1,151,718,569
42	-	-	-	-37,477,999	-28,108,499	-28,108,499	-3,621,488	-1,155,340,057
43	-	-	-	-37,477,999	-28,108,499	-28,108,499	-3,449,037	-1,158,789,093

Daily operation and CO2 is purchase

Table 5.8: Detailed cash flow overview for the project over 44 years

Year	Capital Expenses	Working Capital	Depreciation	Net Profit	IAT	OCF	DCF	NPV
0	251,116,071	12,555,804	-	-	-	-263,671,875	-263,671,875	-263,671,875
1	-	-	26,506,696	-41,697,929	-51,153,469	-77,660,166	-73,962,063	-337,633,938
2	-	-	26,506,696	-41,697,929	-51,153,469	-77,660,166	-70,440,060	-408,073,997
3	-	-	26,506,696	-41,697,929	-51,153,469	-77,660,166	-67,085,771	-475,159,769
4	-	-	26,506,696	-41,697,929	-51,153,469	-77,660,166	-63,891,211	-539,050,979
5	-	-	26,506,696	-41,697,929	-51,153,469	-77,660,166	-60,848,772	-599,899,751
6	-	-	26,506,696	-41,697,929	-51,153,469	-77,660,166	-57,951,211	-657,850,963
7	-	-	26,506,696	-41,697,929	-51,153,469	-77,660,166	-55,191,630	-713,042,593
8	-	-	26,506,696	-41,697,929	-51,153,469	-77,660,166	-52,563,457	-765,606,050
9	-	-	26,506,696	-41,697,929	-51,153,469	-77,660,166	-50,060,435	-815,666,485
10	-	-	26,506,696	-41,697,929	-51,153,469	-77,660,166	-47,676,605	-863,343,090
11	-	-	-	-41,697,929	-31,273,447	-31,273,447	-18,284,937	-881,628,027
12	-	-	-	-41,697,929	-31,273,447	-31,273,447	-17,414,226	-899,042,253
13	-	-	-	-41,697,929	-31,273,447	-31,273,447	-16,584,977	-915,627,229
14	-	-	-	-41,697,929	-31,273,447	-31,273,447	-15,795,216	-931,422,445
15	-	-	-	-41,697,929	-31,273,447	-31,273,447	-15,043,063	-946,465,508
16	-	-	-	-41,697,929	-31,273,447	-31,273,447	-14,326,726	-960,792,234
17	-	-	-	-41,697,929	-31,273,447	-31,273,447	-13,644,501	-974,436,736
18	-	-	-	-41,697,929	-31,273,447	-31,273,447	-12,994,763	-987,431,499
19	-	-	-	-41,697,929	-31,273,447	-31,273,447	-12,375,965	-999,807,464
20	-	-	-	-41,697,929	-31,273,447	-31,273,447	-11,786,633	-1,011,594,097
21	-	-	-	-41,697,929	-31,273,447	-31,273,447	-11,225,365	-1,022,819,462
22	-	-	-	-41,697,929	-31,273,447	-31,273,447	-10,690,824	-1,033,510,286
23	-	-	-	-41,697,929	-31,273,447	-31,273,447	-10,181,737	-1,043,692,023
24	-	-	-	-41,697,929	-31,273,447	-31,273,447	-9,696,892	-1,053,388,916
25	-	-	-	-41,697,929	-31,273,447	-31,273,447	-9,235,136	-1,062,624,051
26	-	-	-	-41,697,929	-31,273,447	-31,273,447	-8,795,367	-1,071,419,418
27	-	-	-	-41,697,929	-31,273,447	-31,273,447	-8,376,540	-1,079,795,959
28	-	-	-	-41,697,929	-31,273,447	-31,273,447	-7,977,657	-1,087,773,616
29	-	-	-	-41,697,929	-31,273,447	-31,273,447	-7,597,769	-1,095,371,385
30	-	-	108,028,851	-41,697,929	-112,295,085	-220,323,936	-50,977,990	-1,146,349,375
31	-	-	-	-41,697,929	-31,273,447	-31,273,447	-6,891,400	-1,153,240,775
32	-	-	-	-41,697,929	-31,273,447	-31,273,447	-6,563,238	-1,159,804,014
33	-	-	-	-41,697,929	-31,273,447	-31,273,447	-6,250,703	-1,166,054,717
34	-	-	-	-41,697,929	-31,273,447	-31,273,447	-5,953,051	-1,172,007,768
35	-	-	-	-41,697,929	-31,273,447	-31,273,447	-5,669,572	-1,177,677,340
36	-	-	-	-41,697,929	-31,273,447	-31,273,447	-5,399,593	-1,183,076,932
37	-	-	-	-41,697,929	-31,273,447	-31,273,447	-5,142,469	-1,188,219,402
38	-	-	-	-41,697,929	-31,273,447	-31,273,447	-4,897,590	-1,193,116,991
39	-	-	-	-41,697,929	-31,273,447	-31,273,447	-4,664,371	-1,197,781,362
40	-	-	-	-41,697,929	-31,273,447	-31,273,447	-4,442,258	-1,202,223,620
41	-	-	-	-41,697,929	-31,273,447	-31,273,447	-4,230,722	-1,206,454,342
42	-	-	-	-41,697,929	-31,273,447	-31,273,447	-4,029,259	-1,210,483,601
43	-	-	-	-41,697,929	-31,273,447	-31,273,447	-3,837,390	-1,214,320,991

2024 Prices

Table 5.9: Detailed cash flow overview for the project over 44 years

Year	Capital Expenses	Working Capital	Depreciation	Net Profit	IAT	OCF	DCF	NPV
0	251,116,071	12,555,804	-	-	-	-263,671,875	-263,671,875	-263,671,875
1	-	-	26,506,696	-47,347,918	-55,390,961	-81,897,658	-77,997,769	-341,669,644
2	-	-	26,506,696	-47,347,918	-55,390,961	-81,897,658	-74,283,590	-415,953,234
3	-	-	26,506,696	-47,347,918	-55,390,961	-81,897,658	-70,746,276	-486,699,510
4	-	-	26,506,696	-47,347,918	-55,390,961	-81,897,658	-67,377,406	-554,076,915
5	-	-	26,506,696	-47,347,918	-55,390,961	-81,897,658	-64,168,958	-618,245,873
6	-	-	26,506,696	-47,347,918	-55,390,961	-81,897,658	-61,113,293	-679,359,166
7	-	-	26,506,696	-47,347,918	-55,390,961	-81,897,658	-58,203,136	-737,562,302
8	-	-	26,506,696	-47,347,918	-55,390,961	-81,897,658	-55,431,558	-792,993,861
9	-	-	26,506,696	-47,347,918	-55,390,961	-81,897,658	-52,791,960	-845,785,821
10	-	-	26,506,696	-47,347,918	-55,390,961	-81,897,658	-50,278,057	-896,063,879
11	-	-	-	-47,347,918	-35,510,939	-35,510,939	-20,762,511	-916,826,389
12	-	-	-	-47,347,918	-35,510,939	-35,510,939	-19,773,820	-936,600,209
13	-	-	-	-47,347,918	-35,510,939	-35,510,939	-18,832,209	-955,432,418
14	-	-	-	-47,347,918	-35,510,939	-35,510,939	-17,935,437	-973,367,855
15	-	-	-	-47,347,918	-35,510,939	-35,510,939	-17,081,369	-990,449,224
16	-	-	-	-47,347,918	-35,510,939	-35,510,939	-16,267,970	-1,006,717,194
17	-	-	-	-47,347,918	-35,510,939	-35,510,939	-15,493,305	-1,022,210,499
18	-	-	-	-47,347,918	-35,510,939	-35,510,939	-14,755,529	-1,036,966,027
19	-	-	-	-47,347,918	-35,510,939	-35,510,939	-14,052,884	-1,051,018,912
20	-	-	-	-47,347,918	-35,510,939	-35,510,939	-13,383,699	-1,064,402,611
21	-	-	-	-47,347,918	-35,510,939	-35,510,939	-12,746,380	-1,077,148,992
22	-	-	-	-47,347,918	-35,510,939	-35,510,939	-12,139,410	-1,089,288,401
23	-	-	-	-47,347,918	-35,510,939	-35,510,939	-11,561,343	-1,100,849,744
24	-	-	-	-47,347,918	-35,510,939	-35,510,939	-11,010,803	-1,111,860,547
25	-	-	-	-47,347,918	-35,510,939	-35,510,939	-10,486,479	-1,122,347,025
26	-	-	-	-47,347,918	-35,510,939	-35,510,939	-9,987,123	-1,132,334,148
27	-	-	-	-47,347,918	-35,510,939	-35,510,939	-9,511,545	-1,141,845,693
28	-	-	-	-47,347,918	-35,510,939	-35,510,939	-9,058,615	-1,150,904,308
29	-	-	-	-47,347,918	-35,510,939	-35,510,939	-8,627,252	-1,159,531,560
30	-	-	108,028,851	-47,347,918	-116,532,577	-224,561,427	-51,958,450	-1,211,490,010
31	-	-	-	-47,347,918	-35,510,939	-35,510,939	-7,825,172	-1,219,315,182
32	-	-	-	-47,347,918	-35,510,939	-35,510,939	-7,452,545	-1,226,767,726
33	-	-	-	-47,347,918	-35,510,939	-35,510,939	-7,097,662	-1,233,865,388
34	-	-	-	-47,347,918	-35,510,939	-35,510,939	-6,759,678	-1,240,625,066
35	-	-	-	-47,347,918	-35,510,939	-35,510,939	-6,437,788	-1,247,062,854
36	-	-	-	-47,347,918	-35,510,939	-35,510,939	-6,131,227	-1,253,194,081
37	-	-	-	-47,347,918	-35,510,939	-35,510,939	-5,839,264	-1,259,033,344
38	-	-	-	-47,347,918	-35,510,939	-35,510,939	-5,561,204	-1,264,594,548
39	-	-	-	-47,347,918	-35,510,939	-35,510,939	-5,296,384	-1,269,890,932
40	-	-	-	-47,347,918	-35,510,939	-35,510,939	-5,044,176	-1,274,935,109
41	-	-	-	-47,347,918	-35,510,939	-35,510,939	-4,803,977	-1,279,739,084
42	-	-	-	-47,347,918	-35,510,939	-35,510,939	-4,575,216	-1,284,314,300
43	-	-	-	-47,347,918	-35,510,939	-35,510,939	-4,357,348	-1,288,671,649

CH_4 profitability

Table 5.10: Detailed cash flow overview for the project over 44 years (2024 Prices Scenario)

Year	Capital Expenses	Working Capital	Depreciation	Net Profit	IAT	OCF	DCF	NPV
0	72000000	3600000	-	-	-	-75600000	-75600000	-75600000
1	-	-	7600000	18999899.01	8549924.26	949924.26	904689.77	-74695310.23
2	-	-	7600000	18999899.01	8549924.26	949924.26	861609.30	-73833700.93
3	-	-	7600000	18999899.01	8549924.26	949924.26	820580.29	-73013120.63
4	-	-	7600000	18999899.01	8549924.26	949924.26	781505.04	-72231615.60
5	-	-	7600000	18999899.01	8549924.26	949924.26	744290.51	-71487325.08
6	-	-	7600000	18999899.01	8549924.26	949924.26	708848.11	-70778476.98
7	-	-	7600000	18999899.01	8549924.26	949924.26	675093.44	-70103383.54
8	-	-	7600000	18999899.01	8549924.26	949924.26	642946.13	-69460437.41
9	-	-	7600000	18999899.01	8549924.26	949924.26	612329.65	-68848107.76
10	-	-	7600000	18999899.01	8549924.26	949924.26	583171.09	-68264936.67
11	-	-	-	18999899.01	14249924.26	14249924.26	8331635.59	-59933301.09
12	-	-	-	18999899.01	14249924.26	14249924.26	7934891.03	-51998410.05
13	-	-	-	18999899.01	14249924.26	14249924.26	7557039.08	-44441370.97
14	-	-	-	18999899.01	14249924.26	14249924.26	7197180.08	-37244190.90
15	-	-	-	18999899.01	14249924.26	14249924.26	6854457.22	-30389733.68
16	-	-	-	18999899.01	14249924.26	14249924.26	6528054.49	-23861679.19
17	-	-	-	18999899.01	14249924.26	14249924.26	6217194.75	-17644484.44
18	-	-	-	18999899.01	14249924.26	14249924.26	5921137.86	-11723346.58
19	-	-	-	18999899.01	14249924.26	14249924.26	5639178.91	-6084167.67
20	-	-	-	18999899.01	14249924.26	14249924.26	5370646.59	-713521.08
21	-	-	-	18999899.01	14249924.26	14249924.26	5114901.51	4401380.43
22	-	-	-	18999899.01	14249924.26	14249924.26	4871334.77	9272715.20
23	-	-	-	18999899.01	14249924.26	14249924.26	4639366.45	13912081.65
24	-	-	-	18999899.01	14249924.26	14249924.26	4418444.24	18330525.88
25	-	-	-	18999899.01	14249924.26	14249924.26	4208042.13	22538568.01
26	-	-	-	18999899.01	14249924.26	14249924.26	4007659.17	26546227.18
27	-	-	-	18999899.01	14249924.26	14249924.26	3816818.26	30363045.44
28	-	-	-	18999899.01	14249924.26	14249924.26	3635065.01	33998110.45
29	-	-	-	18999899.01	14249924.26	14249924.26	3461966.67	37460077.12
30	-	-	7600000	18999899.01	-42450075.74	-118050075.7	-27314125.34	10145951.79
31	-	-	-	18999899.01	14249924.26	14249924.26	3140105.83	13286057.61
32	-	-	-	18999899.01	14249924.26	14249924.26	2990576.98	16276634.59
33	-	-	-	18999899.01	14249924.26	14249924.26	2848168.55	19124803.14
34	-	-	-	18999899.01	14249924.26	14249924.26	2712541.48	21837344.62
35	-	-	-	18999899.01	14249924.26	14249924.26	2583372.84	24420717.45
36	-	-	-	18999899.01	14249924.26	14249924.26	2460355.08	26881072.54
37	-	-	-	18999899.01	14249924.26	14249924.26	2343195.32	29224267.85
38	-	-	-	18999899.01	14249924.26	14249924.26	2231614.59	31455882.44
39	-	-	-	18999899.01	14249924.26	14249924.26	2125347.23	33581229.66
40	-	-	-	18999899.01	14249924.26	14249924.26	2024140.21	35605369.88
41	-	-	-	18999899.01	14249924.26	14249924.26	1927752.59	37533122.46
42	-	-	-	18999899.01	14249924.26	14249924.26	1835954.84	39369077.30
43	-	-	-	18999899.01	14249924.26	14249924.26	1748528.42	41117605.72